Investigation of the relationship between the high frequency dynamic behavior of tread compound with wet grip performance

Thesis submitted in partial fulfillment

of the requirements for the

award of the degree of

Master of Technology

In

Polymer Technology

Under the joint guidance of Cochin University of Science & Technology

& Apollo Tyres Ltd.

Samson David

Roll # – 95301005

April, 2012

DEPARTMENT OF POLYMER SCIENCE AND RUBBER TECHNOLOGY

COCHIN UNIVERSITY OF SCIENCE AND TECHNOLOGY
COCHIN-682 022, KERALA, INDIA

09.04.2012

C E R T I F I C A T E

This is to certify that the project entitled "**Investigation of the relationship between the high frequency dynamic behavior of Tread compound with wet grip performance**" is a report of original work carried out by **Mr. Samson David,** M.Tech. student, Department of Polymer Science and Rubber Technology, Cochin University of Science and Technology under the supervision of Mr. S.K.P. Amarnath., Head, Advanced Tyre Research, Apollo Tyres Ltd., Limda, Gujarat during 1st July, 2011 to 6th April 2012. No part of the work reported in this project has been presented for any other degree from any other institution.

HEAD OF THE DEPARTMENT

apollo

April 6, 2012
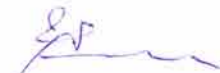
TO WHOMSOEVER IT MAY CONCERN

This is to certify that **Mr. Samson David,** a full time student of M.Tech, Department of Polymer science & Rubber Technology, Cochin University of Science & Technology , Kerala. He has successfully completed his project from 01st July 2011 to 06th April, 2012 at Apollo Tyres Ltd., Limda, Baroda Plant.

He has prepared report on:

- **Investigation of the relationship between the high frequency dynamic behavior of Tread compound with wet grip performance**

We found him to be sincere, hard working and punctual. We wish him all the best in his future endeavour.

For **Apollo Tyres Ltd.**

(Y S D Pawar)
HEAD– HR

Dedicated to my wife & our family

Investigation of the relationship between the high frequency dynamic behavior of tread compound with wet grip performance

Details of project guides and assistance

Guide from Institution: Dr. Professor K E George
Department of Polymer Science and Rubber Technology
Cochin University of Science & Technology

Guides from Industry: Mr. S.K.P Amarnath
Head – Advanced Tyre Research
Apollo Tyres Ltd.

Dr. Rajesh Babu
Associate Manager – Advanced Tyre Research
Apollo Tyres Ltd.

This project work is carried out at Apollo Tyres Ltd.

Project Duration: July 2011 – April 2012

Thesis prepared by: Samson David
Reviewed and corrected by Dr. Rajesh Babu & Professor Dr. Rani Joseph
Email@ samson.david@cusat.ac.in
www.samsondavid.yolasite.com

Contents

`References included at the end of each chapter.

Chapter 1

Introduction

1.1 Genesis of pneumatic tires

Since the invention of pneumatic tires in late 1880s by John Boyd Dunlop, the performance optimizations of the tires were always considered. They very quickly replaced the solid tires, which inflicted increasingly severe punishment on vehicle mechanics and was a source of discomfort for passengers as the drive power and speeds became greater. Greater comfort however was not the only improvement, since the grip ensured by pneumatic tyres also proved to be vastly superior to that of solid tyres.[1]

By 1911, the Hardman Company was successful to produce the tire with the combination of inner tube. Latest major tire research development focuses on the reduction of fuel consumption of the vehicles and an enhanced tire mileage. So the tire industry concentrates on the manufacture and development of low rolling resistance tires. Part of the kinetic energy developed by a vehicle has to be absorbed by the suspension system, the brakes and the tyres during cornering and braking. Where the car meets the road, there are only the vehicle's tyres to ensure the ultimate contact patch. The mechanics of grip are to be explained by the astonishing viscoelastic properties of the tire's rubber which within the contact patch produce a host

of physical phenomena that strive to counteract any untimely skidding over the road surface.[2]

1.2 Background

Vehicle stability and control throughout all the seasons during driving conditions are major prerequisites for the passengers. The road traffic safety and user comfort are the major aspects the industry focus on. UN in its 66th session on 'Global road safety crisis' reveal the statistics on road accident causalities. Nearly 1.3 million people in the world die each year of road crashes, 90 percent of them in low- & middle-income countries. Another 20 to 50 million people suffer serious injuries. Road traffic injuries are also the leading cause of death for

Figure 1: UN Tag of Decade of Action for Road safety

people from 10 to 24 years of age. Figure 1 shows the UN tag of Decade of Action for Road safety. Significant numbers of road traffic fatalities and injuries can be prevented by addressing the leading causes, which include excess speed, poorly designed and inadequately maintained roads, unsafe infrastructure and vehicles, etc… Most of the grievances of road accidents are due to the tire-road grip adequacy. To address these exacerbating safety grievances, UN launched worldwide 'decade of action for road safety 2011-2012' In the context of the Decade of Action for Road Safety 2011-2020, governments around the world have been encouraged to develop national plans for the Decade, as a complement to any current national road safety strategy which may be in place.[3]

Tyres are characterized by a number of parameters which are interrelated. Improving one parameter such as rolling resistance may have an adverse impact on other parameters such as wet grip, while improving wet grip may have an adverse impact on external rolling noise. The European Union (EU) introduced a tire regulation label for all tires as of November 2012, see figure 2. The label focuses on three aspects of the tire: such as fuel efficiency, wet grip and external rolling noises, aiming to increase the safety, and the economic and environmental efficiency of road transport by promoting fuel-efficient and safe tyres with low noise levels.[4]

This labeling indicates:

- The fuel efficiency class (letter A to G, A - the best, G - the worst);
- The wet grip class (letter A to G); at this stage the Regulation only provides classification for wet grip performance for C1 tyres, but intends to introduce a classification for C2 tyres and eventually C3 tyres once tests are available;
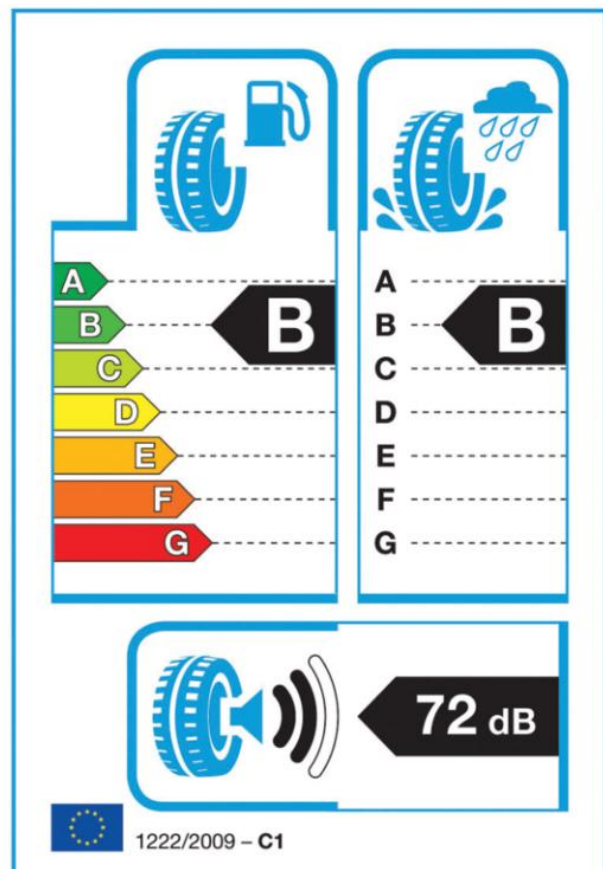- The external rolling noise measured value (in decibels).

Figure 2: EU labeling of Tyres

The tire regulation aims at both improving consumer awareness and forcing tire manufacturers to improve these three aspects of tires. Although there is a possible trade-off between the individual aspects, this thesis focuses mainly on wet skid resistance. So for a sustainable growth, sincere efforts on environmental protection, safety and pollution hazards need to be mandatorily evaluated regularly.

One of the significant aspects in the development of new tire compounds is the correlation between the dynamic mechanical properties of the rubber, measured on laboratory scale, and on the actual tire performance. Considering the current situation the upper and lower control limits are being narrowed for user quality acceptance. The use of elastomers and additives for tire compounding were always been refined since its commercialization. The modern trend is to reduce the use of non-recyclable hydrocarbon resources and to incorporate greener resources.

The rolling resistance (RR) contributes around 20 -30% of the resistance to the forward motion of a passenger car. This will account 15 – 20% excess consumption of fuel to overcome it. Eventually any reduction in RR leads to efficient fuel usage by reducing the consumption by 4 – 6%.

Hysteresis with in the tire fabrics and elastomer is the major contribution to rolling loss and is responsible for 80 – 90% of the total loss. Elastomer modification by optimizing the viscoelastic behaviour is an effective way to reduce the rolling loss. The external friction losses; due to tire slippage between the road and tread; and also the tire internal friction contributes to the total loss.

Skid resistance is also an inevitable property of tire tread on the pavement. Skid resistance of pavement is the opposing force developed at the tire pavement contact area. It is the force that resists the tire sliding on pavement surfaces. It has got two major components: adhesion and hysteresis. Adhesion results from the shearing of molecular bonds formed when the tire rubber is pressed into close contact with pavement surface particles. Hysteresis results from energy dissipation when the tire rubber is deformed when passing across the asperities of a rough surface pavement.

1.3 Basic terminology

1.3.1 Tyres

The invention of the wheel is considered to be one of the most important ever. The first solid wheels where replaced by spoke wheels which allowed for lighter vehicles; their basic design, however, has not been changed for ages. The introduction of pneumatic tyres in the late nineteenth century led to a leap forward in providing comfort by enveloping small obstacles on the road. Since then, pneumatic tyres have been improved in construction and geometry. These tyres are reffered to as bias-ply or diagonal tyres, radial tyres have become more popular, in which the plies are laid at alternate angles of less than 90°. Since the 1960s, radial tyres have become more popular, in which the ply layers are laid at 90° with respect to the centr line of the tread. These layers are reffered to as carcass. On top of the radial carcass diagonal belts are placed at angles between 20 and 30° for more rigidity and better performance. Meanwhile, tubeless tyres which do not require a separate butyl rubber inner tube were introduced and have

improved safety. Nowadays, the aspect ratio of the tyre – the height of the sidewalls to the tyre width – tends to decrease. Thuis change is driven by an increased vehicle power and the ibcreasing importance of design. It also provides better handling on dry roads. The importance of tyre design in the consumer market is reflected in tread pattern types as well. The tread pattern was very simple at the introduction of the pneumatic tyre. Nowadays, complex tread patterns aer available for different applications, from which the summer, winter and all-season tyres are the most well known. These tyres differes not only in tread pattern, but also in rubber compound. For instance, winter tyres consists of a tread rubber compound which is softer than summer tyres, even at low temperatures. Moreover, special tyres have been developed for trucks, trailers and agricultural vehicles.[5]

The main objectives of the tyre are: (i) to carry the weight of the vehicle, (ii) to transmit accelerationa dn braking forces from tyre towards road and (iii) to provide comfort and attenuate unwanted vibrations. These tyre characteristics result in different requirements which are considered important for the evaluation of tyre quality:

- **S**afety: braking and acceleration on different surfaces at different conditions, including aquaplaning;
- **H**andling: tyre performance under slip angles during steering and the tyre characterestics at high speed;
- **D**urability: economic lifetime and tyre mileage;
- **E**nvironment: the use of energy resources during full life cycle, fuel efficiency and rolling resistance;
- **N**oise Vibration and Harness (NVH): mechanical and acoustical comfort for passengers and external tyre/road noise

A modern tyre has a complex geometry which consists of over ten different components with special compounds. A typical construction of a radial tyre is presented in figure 3. The tread (1-2) and sidewalls (3) are the two main rubber assemblies which are visible from outside. The inside of the tyre consists of multiple layers (from inside to outside): an inner liner (11) protects the tyre from depressurizing, the radial textile carcass layers (7-8) and steel belt layers (5) provide the tyre stiffness, and a NOH nylon overhead or cap ply layer (4) prevents the belt from moving outward and protects th e tread. The tread layer on top consists of an under/base (2) and an upper/cap (1) compound; the tread pattern is embedded in the latter. The bead wires (10) and bead filler strip or apex (9) provide stiffness at the tyre edges in order to mount a tyre on a rim. The tyre is connected to the rim by a rim cushion or rim band (12). The requirements of a tyre, combined with complex toroidal geometry and material behaviour, makes the optimization of tyres a hard issue and leads to performance compromises.[6]

1 Tread Cap
2 Tread Base
3 Sidewall
4 Cap ply
5 Steel belts
6 Belt edge cushion
7 Radial textile carcass 2
8 Radial textile carcass 1
9 Bead filler strip
10 Bead wire core
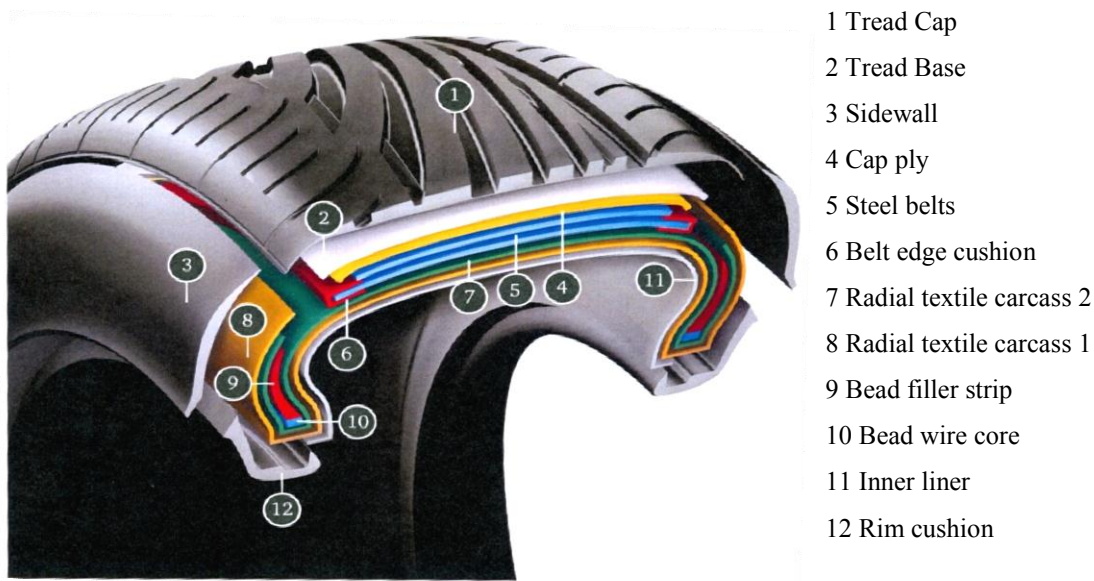11 Inner liner
12 Rim cushion

Figure 3: Cross section of a radial tyre

Tyres are labelled according to, for instance, 245/45R18 98W, in which 245 denotes the tyre section width [mm], 45 the aspect ratio, R the radial tyre construction, 18 the rim diameter [inches], 98 the load index and W the speed rating symbol and also there is more information available on the side wall of the tyre regarding the operational and inflation.

1.3.2 Road surfaces

Systematic paving of road surfaces dates back to the Roman Empire, when cobble stones were used to pave the road. Usually the roads consisted of compacted soil, sometimes reinforced with gravel. From the late nineteenth century concrete pavements, this consists of a mixture of sand and stones with a binder, started to get more widely used. The formerly popular cement concrete, in which cement is used as binder, has been replaced by asphalt concrete, where bitumen is used as binder. Hence, in this thesis, frictional study is based on the asphalt concrete substrate.

A road consists of several bottom layers of sand and gravel, and a top layer which is referred to as road surface. The main objectives of the road surface are: (i) to provide friction between tyre and road, (ii) to provide comfort and (iii) to provide drainage for fluids. Nowadays, wet grip is becoming more important aspect which is been governed by the road texture. The majority of the modern roads are made of a mixture of stones, sand, filler and binder. This binder has to provide adhesion on the concrete mixture itself and between the road surface and the base surface.

Asphalt concrete can be characterized by texture and porosity. Texture is the deviation of the road surface with respect to a planar surface. In a spatial

frequency domain, texture can be presented as a texture amplitude as a function of the road wavelength. Porosity refers to air voids that exist in the pavement providing drainage of water, as well as sound absorption. Some examples of dense road surfaces are Dense Asphalt concrete (DAC), Stone Mastic Asphalt (SMA) and ISO asphaltm a standardised pavement according to ISO 10844. Porous pavements are, for example, single and double layered Porous asphalt Concrete (PAC). Other types of pavements consist of thin layered asphalt and surface dressings. A standard texture of road surface is used as the substrate for friction studies, discussed further.[6]

1.3.3 Grip

Grip is a general safety requirement for any vehicle, whatever the conditions may be, in winter or summer, in the dry or in the wet, on rough or smooth road surfaces, out on the motorway at high speed or on country roads.

If there were no such thing as grip, cars just would not be able to move at all. The wheels would spin and the driver would not be able to budge the vehicle. Even on a straight road and at steady speed, there is no alternative to grip. This is because a moving vehicle has to deal with natural forces, such as the banking, the slope or the unevenness of the road, or rolling resistance, which are constantly trying to slow the vehicle down or push it off its path. However it is only during cornering or braking that a driver or passenger is really aware of grip, because the vehicle has to be steered or speed has to be reduced without skidding, even on a wet road. In all circumstances, grip and safety go together. As the only contact point between the vehicle and the road, the tyre ensures two fundamental functions. It gives the vehicle its

directional stability, which the driver needs to steer it. The tyre acts as a transmission component for brake and drive torque.

Two paradoxes are contained in the ability of the tyre to move and yet to grip at the same time.

Motionless yet moving!

The tyre contact patch of a vehicle travelling at constant speed does not move in relation to the road surface! In order to fully apprehend this first paradox, it must be remembered that before
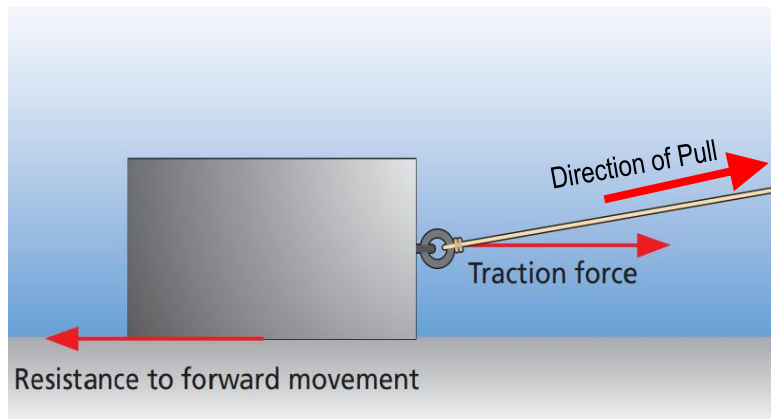

Figure 4: Development of frictional forces at the interface of surfaces

the wheel was invented, men used sleighs and the load was dragged along the ground. Figure 4 shows the frictional forces developed at the interfaces. There was a great deal of resistance to forward movement unless the sleigh was able to slide easily over snow, ice or wooden rollers. Friction was high because the movement over the ground was equal to the speed at which the mass travelled.

The wheel produced a technological revolution:

- Movement was no longer related to a load being dragged directly over the ground, but only to an axle hub.
- At any given time the contact point on the wheel was motionless with respect to the ground, since instantaneous horizontal speed was zero.

Figure 5 shows the trajectory of the point of contact on rotation of the wheel.

The above two features apply to any wheel, although the pneumatic tyre has transformed the old wooden wheel or the
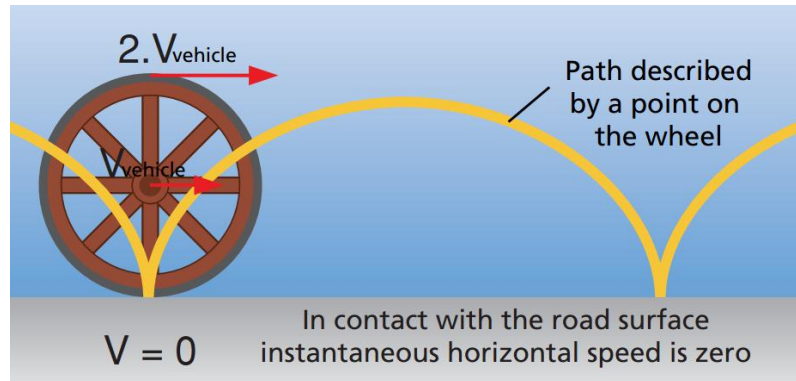

Figure 5: Trajectory of point of contact of a hard wheel on rotation

metal one, because it deflects and so flattens out on the road surface. There is no longer just a contact line across the width of the tyre since the tyre spreads out into a contact patch where the tread blocks are laid down and lifted off like caterpillar tracks.

Furthermore, even though the flattening of the contact area constantly produces micro-movements between the tread blocks and the road surface, the contact area does not move – it changes, as one contact area continuously
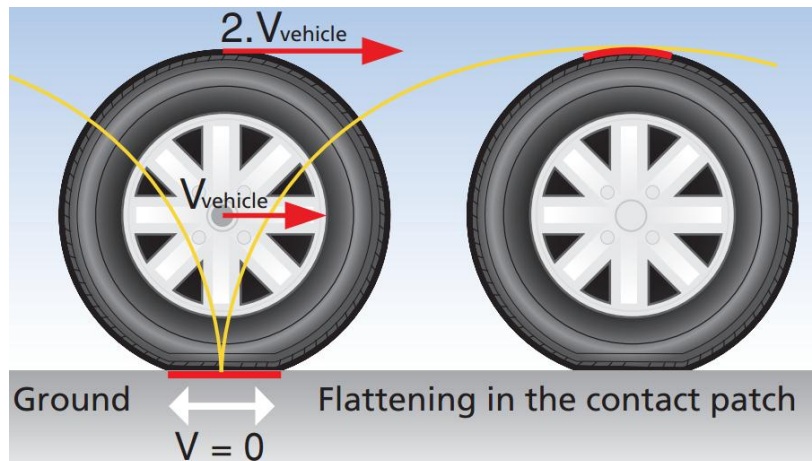

Figure 6: Contact patch of a tyre in motion on the road

replaces the previous one. Figure 6 shows the trajectory of a

pneumatic tyre in motion. It is only when the vehicle brakes, accelerates or corners that the contact area and the road begins to move in relation to each other: this relative movement is known as slippage.

Slippage means no skidding!

Slippage in the contact patch is produced when braking, acceleration or cornering occurs. Here lies the second paradox, which is every bit as surprising as the first: a tyre slips in order not to skid!

Generating grip involves generating friction forces which counteract the vehicle's skidding off the road. However, it must be borne in mind that it is slippage which produces the friction forces of grip. In fact there are two forms of relative movement in the contact patch, micro-movement, commonly known as slippage, which counteracts macro-movement, commonly known as skidding.[1]

1.4 Research objective

The aim of the investigation presented in this thesis is to advance better insight to correlate the wet skid resistance (WSR) with high frequency (0.1 – 10MHz) dynamic mechanical properties of the tread rubber compounds.

The consistency of measurement process for dynamic mechanical properties with high precision and good correlation with tire properties is therefore of main concern. In order to predict WSR or the wet traction, the viscoelastic

behaviour of the rubber materials at high frequencies needs to be known. Therefore the viscoelastic master curves derived from frequency-temperature superposition (WLF) can be used to describe the properties of the materials over a wide frequency range. The material behaviour at very low temperature is significant as it could give higher frequency behaviour (in MHz range).

Understanding the high frequency viscoelastic behaviour of tread compound is therefore essential for studying the wet skid resistance efficiency. Coefficient of friction is found from the linear friction tester (LFT) analysis. LFT is performed at variable slip velocities and loads for different tread compounds. So the WLF transform technique and LFT outputs (friction coefficient) are compared and analyzed for different tread compound to correlate and derive a relation among them.

1.5 Structure of this thesis

The studies described in the present thesis focus on the wet grip performance of tire tread compound design. Chapter 2 gives an overview of the literature survey on mechanisms involved in rubber reinforcement, and in particular with silica, and the role of silane coupling agent and a brief notes on DMA and Linear friction tester apparatus and relevance for this study.

Chapter 3: The experimental details on material used, sample nomenclature and formulation designs, process of mixing and curing, details on physical characterization of the vulcanizate, and detailing on DMA and LFT measurements.

Chapter 4: In this chapter, discussions of the results of rheological properties, physical properties, dynamic mechanical properties, frictional behavior of the compounds, and the correlation of the high frequency dynamic behaviour to the wet frictional behaviour are accompanied.

Chapter 5: Contains the overall conclusions of this thesis and the recommendations on the present work for a sustainable future is mentioned.

References:

1. The tyre grip - Société de Technologie Michelin, 2001

2. Reactive Processing of Silica-Reinforced Tire Rubber: New Insight into The Time- And Temperature-Dependence of Silica Rubber Interaction, By Satoshi Mihara, Ph.D thesis, University of Twente, Enschede, the Netherlands, 2009

3. United Nations-General Assembly, 30 September 2011, Sixty-sixth session, Global road safety crisis, Improving global road safety, Note by the Secretary-General

4. REGULATION (EC) No 1222/2009 OF THE EUROPEAN PARLIAMENT AND OF THE COUNCIL of 25 November 2009

5. Numerical simulation of Tyre/Road noise, Schutte, Jan Henk, Ph.D thesis, University of Twente, Enschede, the Netherlands, 2011

6. U.Sandberg and J.A Ejsmont. Tyre/road noise reference book. Informex, Harg, SE-59040 Kisa, Sweden, first edition, 2002.

Chapter 2

Literature survey

2.1 Silica Mixing methodologies

It is commonly understood in rubber technology that mechanical properties of rubber compounds, such as tensile strength and tear strength, wear resistance, hysteretic loss and resilience, are greatly improved by the inclusion of reinforcing fillers such as carbon black and silica. These differ from non-reinforcing fillers in their specific primary particle and aggregate sizes, their spatial morphology, or "structure", and their surface characteristics – the occurrence of functional groups and resultant surface free energy.[1]

Optimal reinforcing power can be achieved only if the filler is well dispersed in the rubber matrix. The chemical or physical interaction between the filler and the rubber is a further important factor in the reinforcing effect. Traditionally, various carbon blacks have been used as reinforcing fillers[2]. However, the use of silica as filler in rubber affords a number of advantages over carbon black in terms of properties. In tyre treads, silica provides a lower rolling resistance than carbon black at equivalent wear resistance and wet traction[3,4]. Rubber and carbon black, both being hydrophobic substances, are generally easy to mix. But in the case of silica, hydrogen bond interactions between surface silanol groups in agglomerates are very strong by comparison with the potential interactions between the polar siloxane or silanol groups and the commonly non-polar olefinic hydrocarbon

rubbers. These hydrogen bond interactions make it very difficult to mix silica with rubber. Bifunctional organosilane coupling agents are commonly used to chemically modify the surface of the silica in order to enhance interaction with hydrocarbon rubbers. Remarkable improvements in the mechanical properties of the silica-reinforced rubber vulcanizate are obtained, such as improvements in the Young's modulus, tensile strength and elongation at break, lower tanδ at 60 °C and consequently lower heat build-up in the tyre[5,6].

In normal practice the silica, coupling agent and rubber are introduced simultaneously into the internal mixer. A number of chemical reactions are initiated during mixing:

- Bonding of the organosilane to the silica surface;

- Reaction between the organosilane and the rubber polymer.

 The organosilane coupling agents which are currently most widely used for tyre applications is bis(triethoxysilylpropyl) tetrasulphide (TESPT)[7,8]. Originally TESPT was developed as a curing agent[9] and in combination with accelerators such as tetramethylthiuram disulphide (TMTD) and N-cyclohexyl-2-benzothiazole sulphenamide (CBS) TESPT crosslinks silica-containing rubbers without further addition of sulphur, at the same time solving mixing problems encountered with silica. Historically, industry has placed greater emphasis on the coupling role of TESPT because of the greater ease of mixing when it is used for such silica-reinforced systems. But with additional experience the realization came that the cure properties of TESPT must also be considered[10-22].

The specific reaction of TESPT with silica has been studied by Görl et al.[18, 23], who concluded that initially a single bond with the silica surface is formed between one ethoxysilyl group of the coupling agent and a silanol group of the silica (primary reaction). This primary reaction is commonly understood to be followed by further condensation reactions between pairs of neighbouring silane molecules which are already bound to the silica surface (secondary reaction). The energy of activation for both reactions, the primary and the secondary, is within the range of 30 - 50 kJ/mol. The primary reaction of the coupling agent during mixing is relatively slow at moderate temperatures of, for eg:, 120 °C, which poses a problem since this temperature is often employed as the dump temperature. In order to achieve shorter reaction times higher batch temperatures are needed. At these elevated temperatures, on the other hand, a third reaction – between the coupling agent and the rubber is prone to occur, giving rise to scorch problems[24].

Depending on time and temperature, TESPT can disproportionate into a mixture of polysulphides whose sulphur chain lengths vary from two to eight sulphur atoms. Whether this disproportionation reaction occurs during mixing or later in processing apparently has little effect on the efficiency of TESPT as a coupling agent[3].

Modern analytical techniques were applied to analyze the reaction products. The link of the TESPT polysulphide group to the rubber was assumed to be brought about by the intermediate addition of accelerators. The authors propose the course of the reaction via an intermediate asymmetric polysulphide, formed by a reaction between the silane and accelerator, e.g. mercapto benzothiazole. In the subsequent reaction, the polysulphide is substituted into the allyl position of the rubber with release of mercapto benzthiazole: Fig. 7 .This reaction subsequently

leads to a covalent bond between rubber and filler, chemically binding the rubber to the filler[1,2] .Proposed reaction mechanism of TESPT with rubber in the presence of a CBS accelerator.
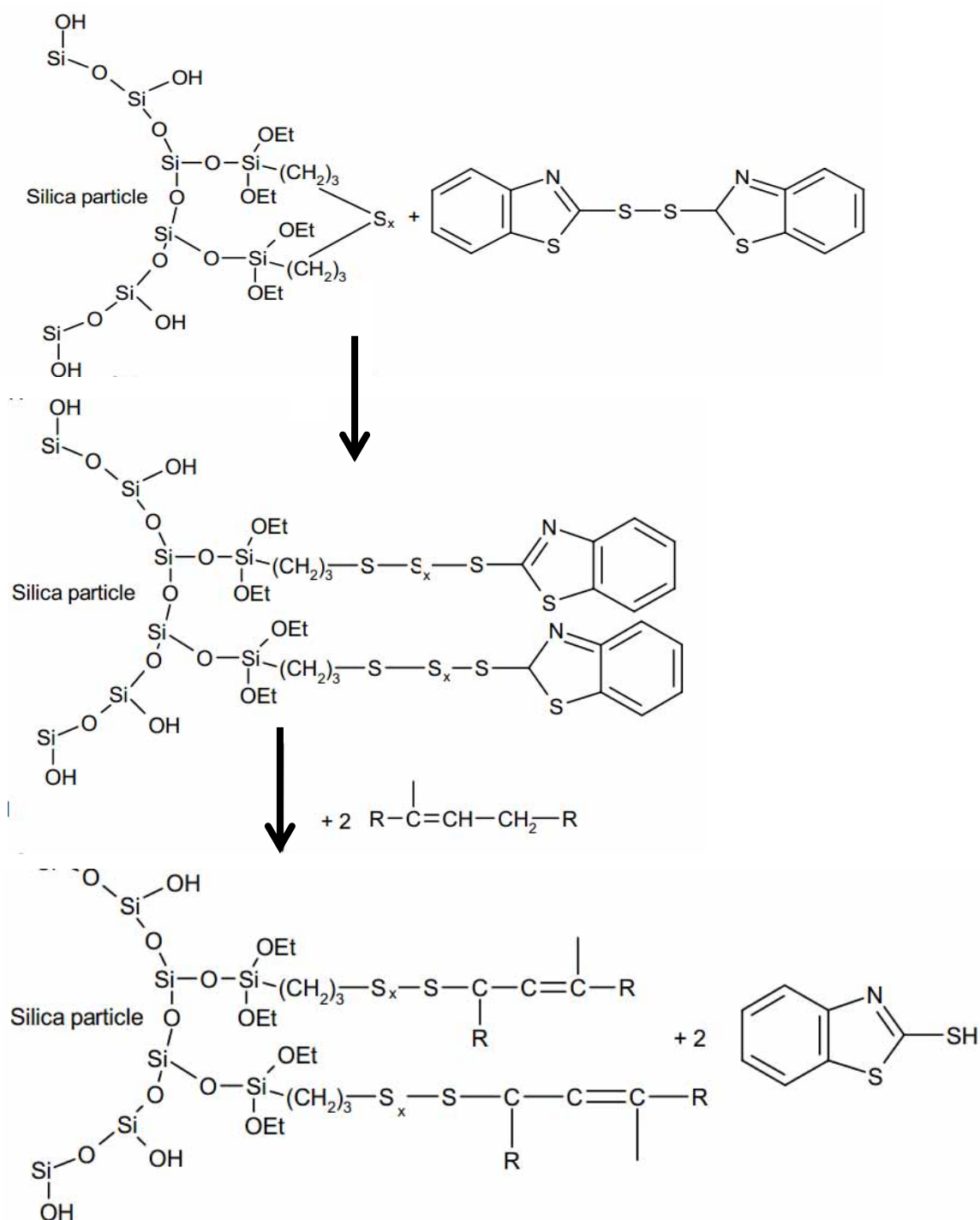

Figure 7: Proposed reaction mechanism of TESPT with rubber in the presence of a CBS accelerator

2.2 DMA for high frequency analysis

In practice, measuring dynamic properties is limited to the accessible frequency range of the instrument. However, the modulus at high frequencies is available via the time-temperature superposition principle. According to this principle, the effect of changing the temperature is the same as applying a shift factor aT to the time scale. The time-temperature superposition for polymeric materials was proposed by Williams, Landel and Ferry in 1955 and is generally referred to as the WLF principle. According to this principle, the horizontal shift factor aT is given by:

$$\log(a \quad \frac{-C_1}{C_2 +}$$

(Where $T_g < T < T_{g+100}$)

Where T is temperature and T_g is the glass transition temperature. The constants C_1 and C_2 vary with the choice of the reference temperature T_{ref}. If the glass transition temperature is taken as the reference temperature, the two constants have almost

Figure 8: Creation of master curve for E' using WLF shifts

universal values for many high diene rubbers: $C_1 = 17.4$ and $C_2 = 51.6$. These values only differ slightly from one polymer system to the other. Master curves were plotted with C_1 and C_2 values thus obtained from DMA.

The high frequency behaviour of the tread compound reveals the wet skid resistance of the material. The tire performance is related to the dynamic
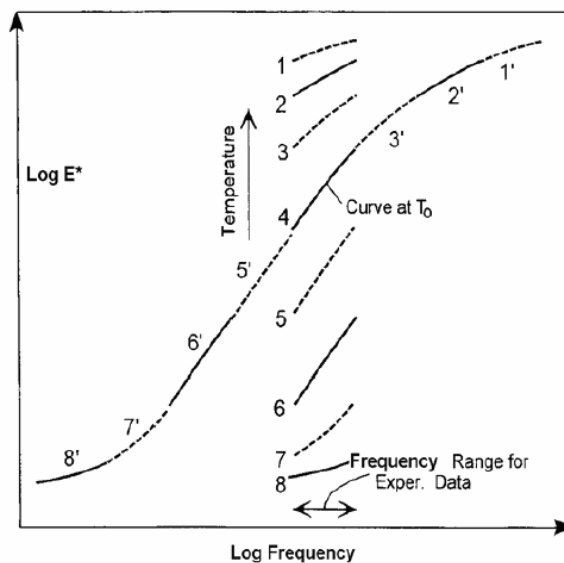
mechanical properties of the material. Rolling resistance is related to the hysteresis. When energy is brought in to the material, it is partly dissipated into the tire material as heat and partly stored elastically. The below figure shows the general trend of frequency response on the storage and loss modulus.

Wet skid is a high frequency phenomenon, in the transition zone between the rubbery and the glassy state, typically in the megahertz region. The position of wet skid on the frequency scale shows, that the glass transition temperature has a strong influence on this property of a tire.
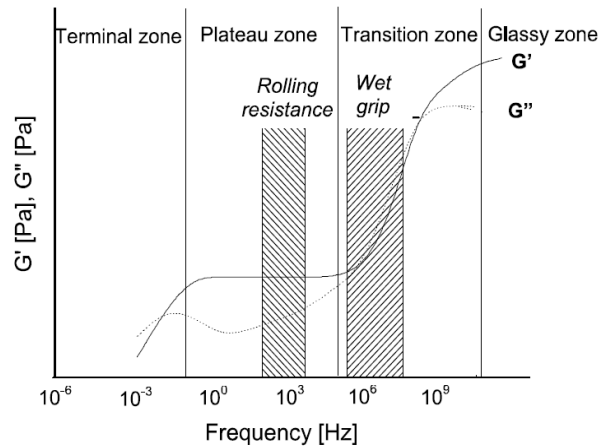
Figure 9: The frequency response of the storage modulus E'& the loss modulus E''

2.3 Friction and LFT for coefficient of friction analysis

Rubber friction differs in many ways from the frictional properties of most other solids. The reason for this is the very low elastic modulus of rubber and the high internal friction exhibited by rubber over a wide frequency region. In particular, there is a marked change in friction at high speeds and low temperatures, where the rubber's response is driven into the so-called glassy region. In this region, the friction shows marked stick-slip and the coefficient of friction depreciates. This proves that the friction force under most normal circumstances is directly related to the internal friction of the rubber.[25-28]

It is widely accepted that there are two principal factors, adhesion and hysteresis, commonly considered to give rise to a frictional force during the sliding of a rigid surface on a flexible elastomer. Assuming a dry, smooth contact with reasonably low shear forces, the total frictional force (F_{TOTAL}) during sliding at an elastomer/rigid interface is considered to arise from the combination of two forces[29.]

$$F_{TOTAL} = F_{ADHESION} + F_{HYSTERESIS}$$

The adhesion term ($F_{ADHESION}$) is a surface effect resulting from the intermolecular interaction between two surfaces [30] and the hysteresis term ($F_{HYSTERESIS}$), sometimes referred to as the deformation contribution, results from the energy lost through the bulk deformation process of a certain volume of rubber [31]. By lubricating the interface (wetting the contact area), can alter either of the two terms and can therefore change their ratio significantly. Fuller and Tabor[32] and Persson[33] have all stated that $F_{ADHESION}$ is negligible in a tyre to wet road contact, and the major contribution to friction is from the hysteresis term alone.[34]

The hysteric component $F_{HYSTERESIS}$ results from the internal friction of the rubber: during sliding the asperities of the rough substrate exert oscillating forces on the rubber surface, leading to cyclic deformations of the rubber, and to energy ''dissipation'' via the internal damping of the rubber. $F_{HYSTERESIS}$ in general, depends on road texture, elastomer viscoelasticity, and contact conditions.[35]

General road texture classification

Generally road pavements are classified according to their texture wavelength. Pavement texture wavelength highly influences on wet grip between the tire tread surface and the pavement. The highly influencing pavement textures are microtextures and macrotextures on the wet skid resistance.
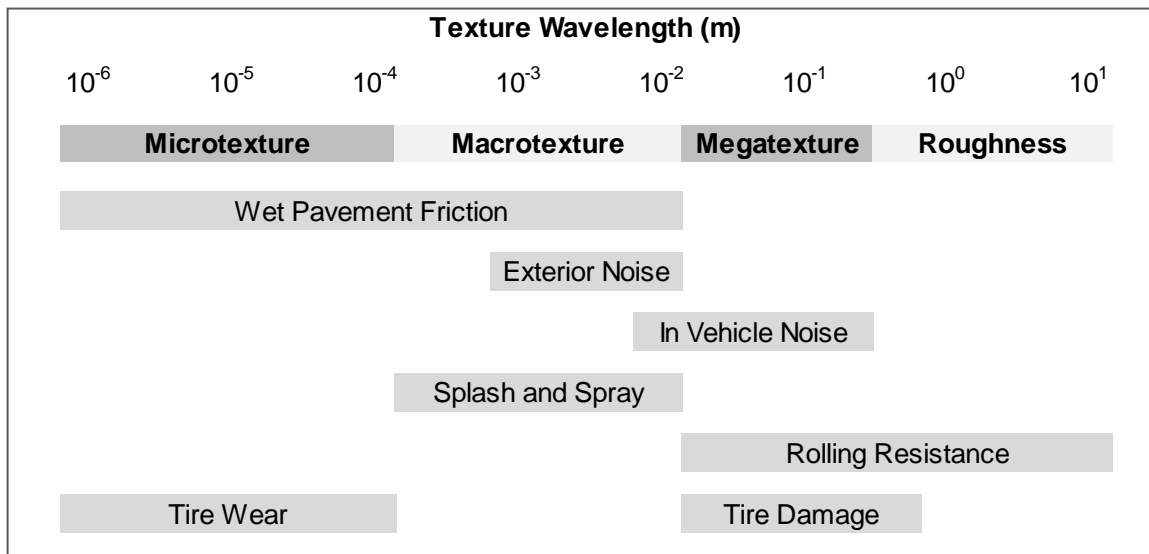

Texture Wavelength (m)

10^{-6}	10^{-5}	10^{-4}	10^{-3}	10^{-2}	10^{-1}	10^{0}	10^{1}

Microtexture	Macrotexture	Megatexture	Roughness

Wet Pavement Friction

Exterior Noise

In Vehicle Noise

Splash and Spray

Rolling Resistance

Tire Wear

Tire Damage

Figure 10: Texture Wavelength (m) influence on surface characteristics

Microtexture refers to irregularities in the surfaces of the stone particles (fine scale texture) that affect adhesion. The magnitude of microtexture depends on initial roughness on the aggregate surface and the ability of the aggregate to retain this roughness against the polishing action of traffic. Microtexture and adhesion contributes to skid resistance at all speeds.

Macrotexture refers to the larger irregularities on the road surface (coarse-scale texture) that effect hysteresis. These larger irregularities are associated with voids between stone particles. Macrotexture is also essential; as it provides escape channels to water during the tire-surface interaction and thus reducing

hydroplaning. Macrotexture and hysteresis are less critical at low speeds; however, as the speed increases a coarse macrotexture is very desirable for safe wet-weather travel.

Two other road surface textures, namely megatexture and roughness (unevenness), are less significant in the generation of wet skid resistance. Microtexture, macrotexture, megatexture, and roughness are the features of the road surface that ultimately influence most tire road interactions including wet pavement skid resistance, noise, splash and spray, rolling resistance, and tire wear

There must be contact between the tyre and the road for grip to be produced. Grip comes from road roughness effects and molecular adhesion[36].

Pavement roughness provides a good overall measure of the pavement condition and is usually computed through the International Roughness Index (IRI). The concept
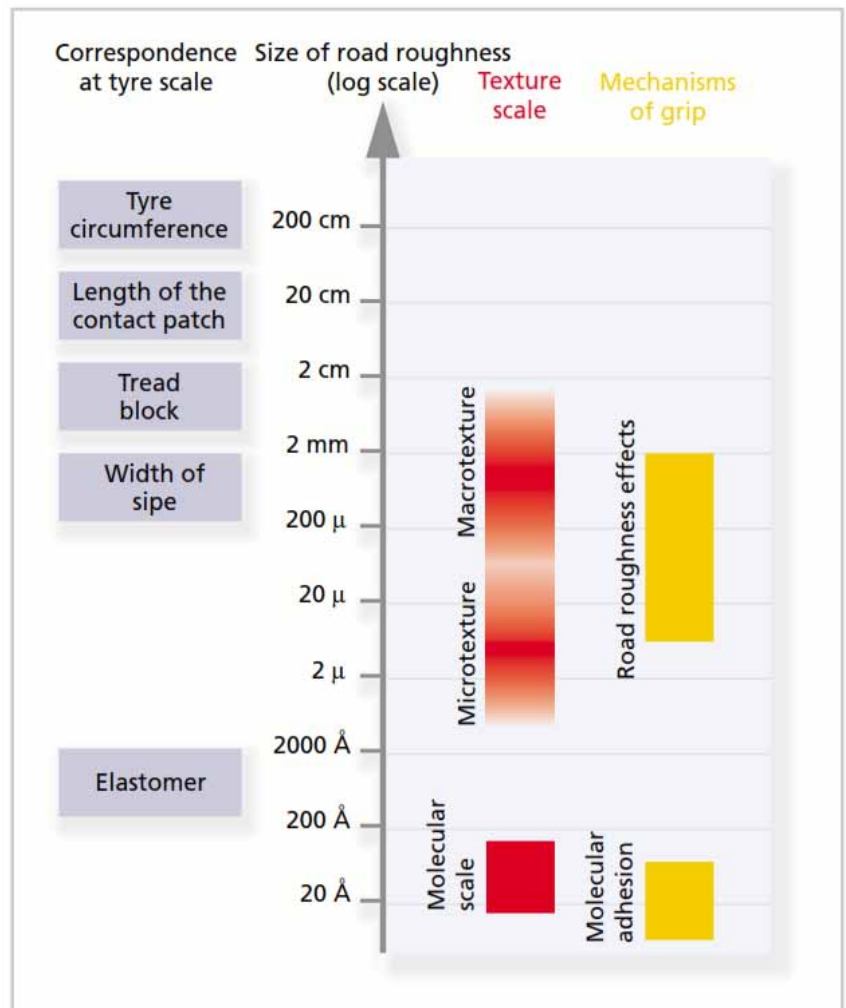
Figure 11: Influence of the road texture on the tyre scale

called the International Friction Index (IFI), is now a standard (ASTM E 1960) and can be calculated from the measurement of pavement macrotexture and wet pavement friction. The IFI model consists of two numbers that describe the skid resistance of a pavement: the speed constant and the friction number.

The table below shows some of the extreme wet skid friction coefficient during braking.

Snow or Ice Conditions	Friction Coefficient
Ice	0.10 - 0.20
New Snow	0.20 - 0.25
Old Snow	0.25 - 0.30
Refrozen Snow	0.30 - 0.40
Chloride-Treated Snow	0.35 - 0.45
Sand-Treated Snow	0.30 - 0.40
Chloride-Sand Mix	0.30 - 0.50

Table 1: Various friction coefficients during braking

In addition to climate and water in the pavement, the potential for a skidding crash depends mainly on the speed of the vehicle (frictional demand increases with the square of the speed), the cornering path, the magnitude of acceleration or braking, and the condition of the vehicle tires, and also the characteristics of the pavement surface.[37]

Road texture depth & Tread strain levels

From recent studies on highways and accidents by DOT - NHSA, it shows that the wet weather crashes are high for sand-patch texture depth less than about 0.5mm. The figure 12 shows the immediate rise in the accident cases in US highways when the texture depth lowers from 0.5mm.
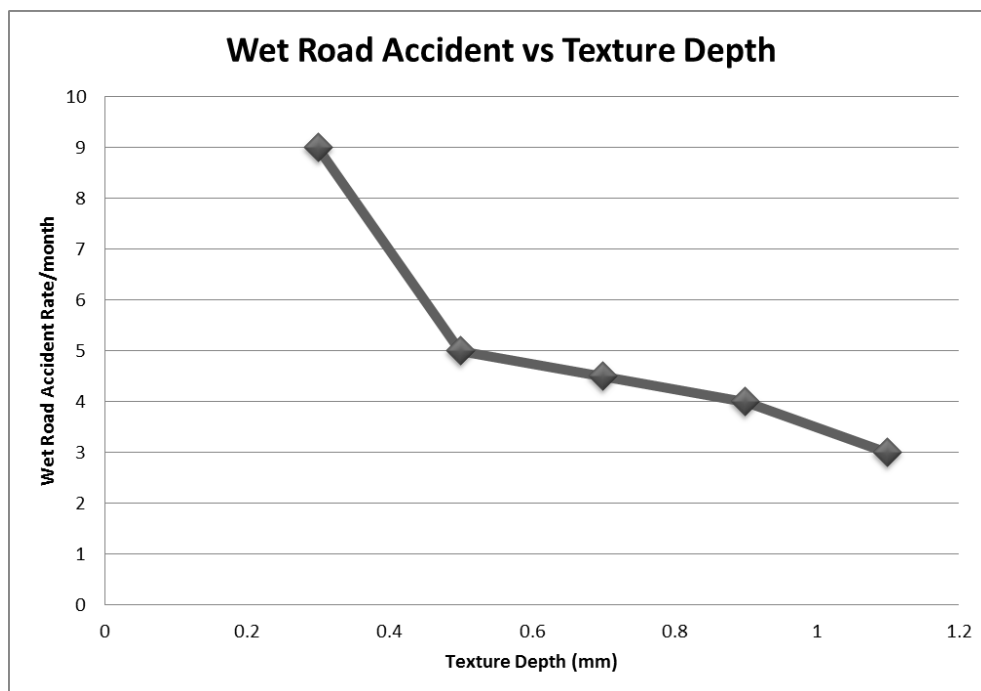
Figure 12: Relationship between wet accident and surface texture depth

From the research it is obvious that the average pavement texture depth lies in the range of 0.8 mm to 1.2 mm. This will give us an understanding that, the tread rubber traces those depth irregularities and get strained in a cyclic fashion with varied frequencies. The excitation over the tire tread is very high during the rolling, acceleration / braking operation on the pavement. So the tread rubber is strained at high frequencies during this excitation at low amplitudes.

Commercially available passenger car tires have a tread depth range of 5mm to 10mm. So the tread portion is traced into the pavement depths during the tire traction. This leads the tire tread portion to be strained through 3 – 10%. Therefore low strain levels and very high frequency should be studied for WSR analysis.

Static and dynamic friction

Friction is typically characterized by the coefficient of friction which is the ratio of the frictional resistance force to the normal force which presses the surfaces together.

$$\mu = F_{horizontal}/F_{normal}$$

Static frictional forces are produced from the interlocking of the surface irregularities of two substrates tends to increase to prevent any relative motion up until some limit where motion occurs. It is that threshold of motion which is characterized by the coefficient of static friction. At lower slip velocities, there creates an instantaneous static fiction which holds on, until it crosses the threshold value of static friction.

When two surfaces are moving with respect to one another, the frictional resistance is deteriorating from the point of motion; this shows the dynamic friction occurrence. The coefficient is typically less than the coefficient of static friction, reflecting the common experience that it is easier to keep something in motion across a horizontal surface than to start it in motion from rest. When coefficients of friction are quoted for specific surface combinations, it is the kinetic coefficient which is generally quoted since it is the more reliable number.

A rolling wheel requires a certain amount of friction so that the point of contact of the wheel with the surface will not slip. There is some loss of energy and some deceleration from friction for any real wheel, and this is sometimes referred to as rolling friction. If the wheel is locked and skidding,

the force of friction is determined by the coefficient of kinetic friction and is usually significantly less.

Linear Friction Tester

Experimental investigations of the sliding behaviour of rubber blocks are performed at Linear Friction Tester (LFT), which is a testing device developed at the Laboratory of the Institute for Mechanics of Materials and Structures at Vienna University of Technology on behalf of Continental AG. A detailed description of the device can be found in.[38]
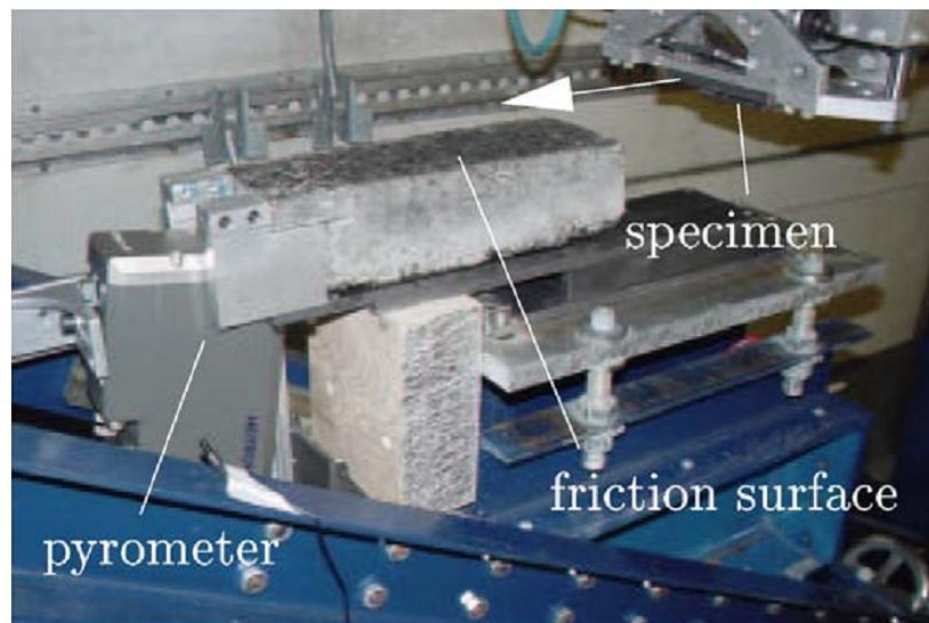
Figure 13: Shows a photo of the LFT specifying its main components

The rubber test specimens are pulled in a displacement-controlled manner over friction surfaces which are considered as self-affine, cut out of real road surfaces. During the sliding motion, the resulting forces in horizontal and vertical direction as well as the displacements in these directions are recorded. The forces allow for the computation of a resulting friction

coefficient. A radiation pyrometer installed at the end of the friction surface serves for temperature measurement at the bottom surface of the test specimens after sliding. Most parameters of the contact model are identified on basis of results from tests at the LFT. The test procedures and the parameter identification processes are documented in the reference[39] in detail.

LFT is capable of testing the samples at various slip velocities. The extreme boundary conditions such as low slip velocity to very high slip velocity could give the real time tire rolling friction and sliding friction. Therefore the results from these test conditions are well suited for the study.

In this investigation, elastomer friction is studied with varying the normal load and sliding velocity. The temperature and the substrate texture is set to be constant throughout the testing. Results are widely in acceptance with the frictional behavior as expected. The coefficient of friction increases to a threshold and then reverses on the increase of the sliding velocity. This shows the phenomenon of static friction and dynamic friction characteristics.
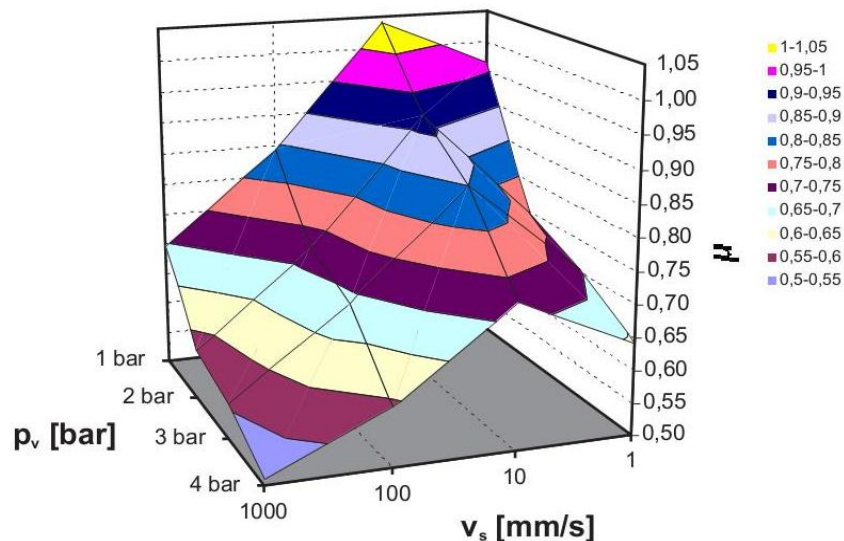
Figure 14: Shows the frictional coefficient values with increasing the sliding velocity.

The test specimen used for LFT measurements is a rectangular prism with dimensions 20x12x80 (mm) (Figure 15). Due to the limitations of the LFT load cell capacity the actual contact area is reduced to 20x20 mm^2.
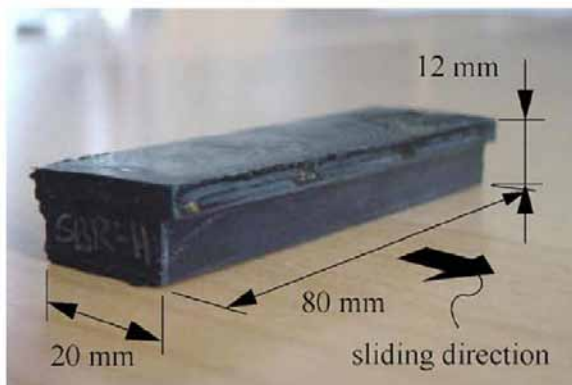
Figure 15: Shows the LFT specimen and its dimensions

Vertical load is applied on the specimen and made to slide on the self-affine substrate. The magnitude of vertical load applied is selected based on the practical significance of unladed vehicle and of a loaded vehicle and the sliding velocity is selected based on the influence of rolling friction and sliding friction phenomenon.
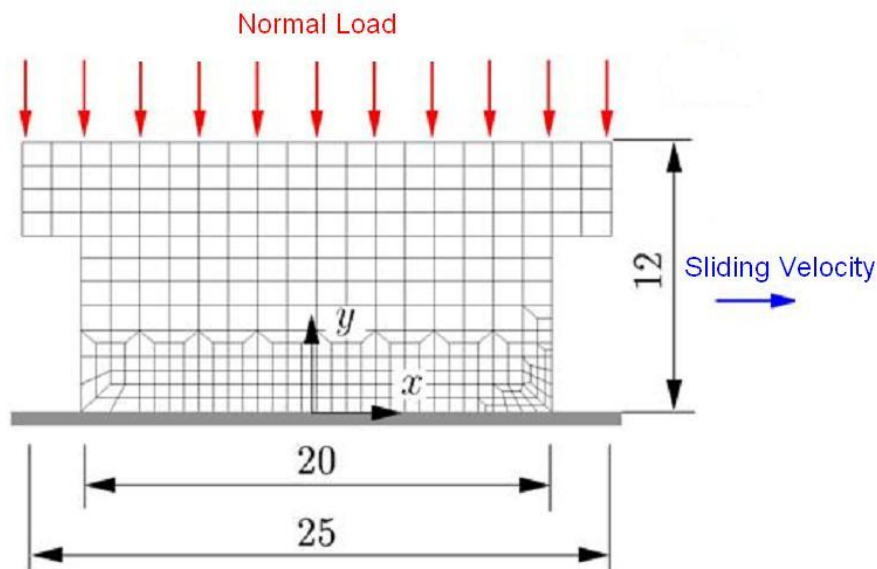
Figure 16: Shows the grid view of the specimen cross section and the application of load and sliding motion

The surface roughness characterization of the LFT substrate is having a RMS deviation of the distribution of the surface height of 0.79mm and an

mean profile depth (MPD) of 1.66mm. The histogram of the substrate texture is shown in figure 17.
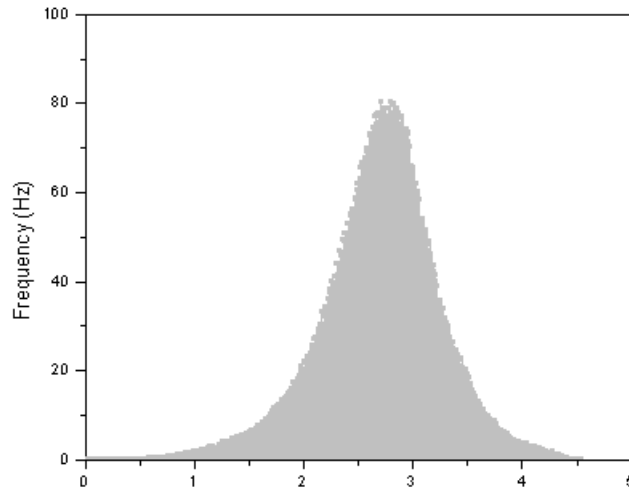
Figure 17: Shows the histogram of the LFT substrate texture

The coefficient of friction between the sliding rubber and the rough road surface is a function of viscoelastic characteristics of elastomer, pavement texture characteristics and interface contact conditions. Interface contact conditions include mainly the temperature influence and the surface impurities such as wet, dry and dusty surfaces. The test temperature is set at 20°C. The interface contact conditions are maintained as dry and wet test conditions. The distinct temperature dependence of many properties of rubber, especially of its stiffness, results in a non-negligible influence of the local temperature rise at the contact surface on the frictional behaviour. The surface temperature after each cycle is recorded using a pyrometer and the rise in the surface temperature from the test temperature is found out. Friction results in detachment of material (elastomer) particles from the contact surface. This process is generally denoted as abrasion or wear. The mass loss of each sample is found for dry condition by summing-up of mass

loss (because of low values for wet condition) for all the sliding velocity variations to each set of vertical load condition.

References:

1. M. J. Wang, S. Wolff and J. B. Donnet, Rubber Chem. Technol., 64, 559 (1991).

2. J. B. Donnet, Kautsch. Gummi Kunstst., 47, 628 (1994).

3. S. Wolff, Tire Sci. Technol., 15, 276 (1987).

4. M. P. Wagner, Rubber Chem.Technol., 49, 703 (1976).

5. E. M. Dannenberg, Rubber Chem. Technol., 48, 410 (1975).

6. Y. Bomal, S. Touzet, R. Barruel, P. Cochet and B. Dejean, Kautsch. Gummi Kunstst., 50, 434 (1997).

7. B. T. Poh and C. C. Ng, Eur. Pol. J., 24, 975 (1998).

8. R. H. Hess, H. H. Hoekje, J. R. Creasey and F. St raim (to PPG Industries), US Pat. 3,768,537 (30-10-1973).

9. S. Wolff, Kautsch. Gummi Kunstst., 30, 516 (1977).

10. F. Thurn and S. Wolff, Kautsch. Gummi Kunstst., 28, 733 (1975).

11. S. Wolff, Kautsch. Gummi Kunstst., 34, 280 (1981).

12. S. Wolff, Rubber Chem. Technol., 55, 967 (1982).

13. S. Wolff, Kautsch. Gummi Kunstst., 36, 969 (1983).

14. S. Wolff, E. H. Tan and J. B. Donnet, Kautsch. Gummi Kunstst., 47, 485 (1994).

15. S. Wolff, U. Görl, M. J. Wang & W. Wolff, Eur. Rubber J.,January,16,1994

16. S. Wolff, Rubber Chem. Technol., 69, 325 (1996).

17. U. Görl and A. Parkhouse, K autsch. Gummi Kunstst., 52, 493 (1999).

18. U. Görl and J. Muenzenberg, Paper No. 38 presented at a meeting of ACS, Rubber Division, Anaheim, California, May 6-9, 1997

19. H. D. Luginsland, Paper No. 74 pr esented at a meeting of ACS, Rubber Division, Chicago, Illinois, April 13-16, 1999

20. H. D. Luginsland, Kautsch. Gummi Kunstst., 53, 10 (2000).

21. H. D. Luginsland, Paper No. 34 pr esented at a meeting of ACS, Rubber Division, Dallas, Texas, April 4-6, 2000

22. A. Hasse and H. D. Luginsland, pr esented at a meeting of International Rubber Conference, Helsinki, Finland, June 12-15, 2000

23. A. Hunsche, U. Görl, H. G. Koban and T. Lehmann, Kautsch. Gummi Kunstst., 51, 525 (1998).

24. J. W. Pohl, Paper No. 100 presented at a meeting of ACS, Rubber Division, Cleveland, Ohio, October 21-24, 1997

25. D.F. Moore, The Friction and Lubrication of Elastomers, Pergamon Press, Oxford, 1972.

26. B.N.J. Persson, Sliding friction, Surf. Sci. Rep. 33 (1999) 83–119.

27. S. Sills, K. Vorvolakos, M.K. Chaudhury, R.M. Overney, Molecular Origins of Elastomeric Friction/Nanotribology: Friction and Wear on the Atomic Scale, Springer Verlag, New York, 2007.

28. A.D. Roberts, Natural Rubber Science and Technology, Oxford University Press, Oxford, 1988, p. 774.

29. D. Tabor, Hysteresis losses in the friction of lubricated rubber, Rubber Chem. Technol. 33 (1960) 142–150.

30. A.D. Roberts, A.G. Thomas, The adhesion and friction of smooth surfaces, Wear 33 (1975) 46–64

31. A.D. Roberts, A guide to estimating the friction of rubber, Rubber Chem. Technol. 65 (1992) 673–686.

32. K.N.G. Fuller, D. Tabor, The effect of surface roughness on the adhesion of elastic

solids, Proc. R. Soc. Lond. Ser. A 345 (1975) 327–342.

33. B.N.J. Persson, Theory of rubber friction and contact mechanics, J. Chem. Phys.

118 (2001) 3840–3861.

34. Influence of interface geometry on rubber friction, P. Gabriel, A.G. Thomas, J.J.C. Busfield*

35. Sliding behaviour of simplified tire tread patterns investigated by means of FEM, K. Hofstetter *, Ch. Grohs, J. Eberhardsteiner, H.A. Mang, Institute for Mechanics of Materials and Structures, Vienna University of Technology,

Karlsplatz 13/202, 1040 Vienna, Austria Received 15 August 2005; accepted 18 January 2006

36. The tyre grip - Société de Technologie Michelin, 2001

37. Incorporating Road Safety into Pavement Management: Maximizing Surface Friction for Road Safety Improvements: David A. Noyce, Hussain U. Bahia

38. Eberhardsteiner J, Fidi W, Liederer W. ExperimentelleBestimmung der adha¨ sivenReibeigenschaften von Gummiproben auf ebenenOberfla¨ chen. KautschukGummiKunststoffe 1998;51(11):773–81 [in German]

39. Hofstetter K, Eberhardsteiner J, Mang HA. Efficient treatment of rubber friction problems in industrial applications by means of the FEM. StructEngMech 2006;22(5):517–39.

Chapter 3

Experimental

3.1 Materials

OE-SSBR (Oil extended solution SBR) VSL 5025-2 with vinyl content 50% and styrene content 25% [Mooney viscosity ML (1+4) @ 100°C =50] supplied by Lanxess International S.A. France and OE-ESBR (Oil extended emulsion SBR) 1783 with styrene content 23.5% [Mooney viscosity ML (1+4) @ 100°C =50] supplied by Kumho petro chemicals, Korea.

These 2 types of elastomers are used in 1:1 ratio for the analysis. ESBR is less expensive because it is easy to produce, so it is widely used. But it is easy to control microstructure & macrostructure in SSBR with
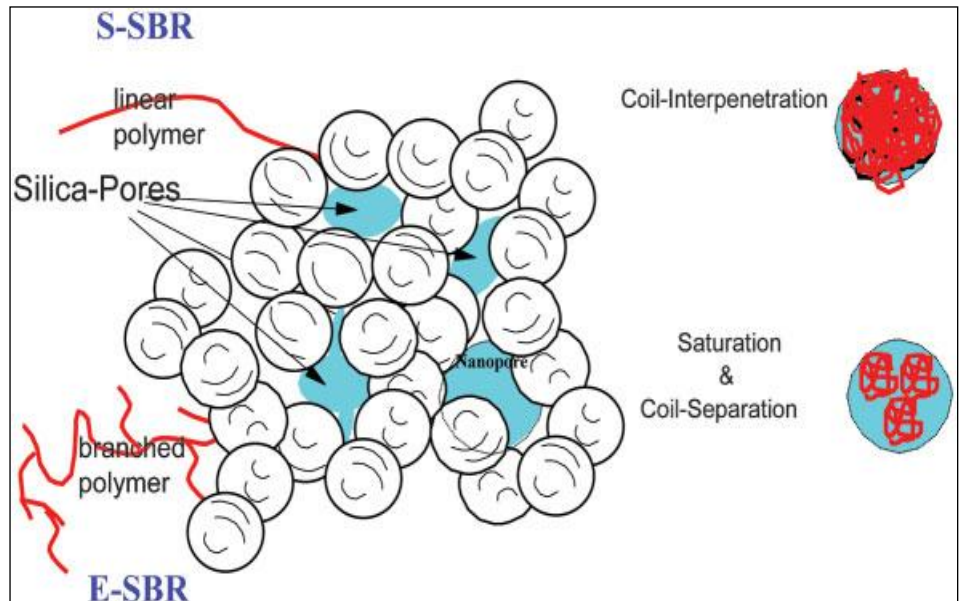
Figure 18: Pictorial representation of ESBR & SSBR in silica mixing

respect to ESBR. SBR is oil-extended because of easy processing. SSBR is relatively more linear with respect to ESBR.

High abrasion furnace black, ISAF (N-220) was obtained from Hi-Tech carbon, Gummidipoondi - India having the following characteristics: Iodine absorption #121g/kg; DBP absorption #114 ml/100g; DBP absorption # (compressed sample)98 ml/100g; nitrogen surface area110.0 m2/g; and tinting strength of 115%.

ULTRASIL 7000 GR (highly dispersible silica) was supplied by Evonic industry, Silane coupling agent X 266 S (blend of the bi-functional sulphur containing organosilane and N 330 type carbon black in the ratio of 1:1 by weight) was supplied by Evonic Degussa GmbH industry; additives[Appendix D] (ZnO, stearic acid, sulphur, CBS, DPG, 6PPD) consumed are quality certified by the R&D team.

3.2 Sample Nomenclature and Formulation

Three sets of formulations varying the silica and carbon black content were considered for the analysis. Elastomer content is not varied and designed as 50% oil extended emulsion SBR and 50% oil extended solution SBR.

Samples are designated as **ES##**; where **'E'** stands for oil extended emulsion SBR; **'S'** stands for oil extended solution SBR and **##** shows the amount of silica content in a total of 100 phr dual phase filler. Detailed formulation is given in Appendix C

Compound design:

Ingredients	ES50	ES75	ES100
VSL5025 O-SSBR	68.7	68.7	68.7
1783 O-ESBR	68.7	68.7	68.7
HD Silica 7000	**46**	**69**	**92**
Silane X266S	**8**	**12**	**16**
N220 – ISAF	**46**	**9.5**	**0**

Table 2: Compound formulation varying the silica – carbon black ratio

3.3 Mixing and Curing

Compounding was done in lab size banbury (FAMM LIMITED, MUMBAI, INDIA) at initial temperature 80°C and a dump temperature of 150 – 155 °C and rotor speed at 50 rpm. Capacity of Banbury was 2100 cc. Three stages of mix were carried out for better dispersion of silica formulations. Master batch was prepared by addition of all the ingredients with rubber except curatives. Each stage of mix was matured overnight. The curatives were finally added to the resulting master batch and were sheeted out in a two roll mill (Santosh Industries, India).

Optimum cure time (OCT) for the compounds were determined by Moving Die Rheometer (MDR 2000 Alpha Technologies, USA) at 160°C for 30 minutes. The sheets were molded at 160°C in compression molding machine (Santosh Industries, India).

3.4 Physical Characterization

3.4.1 Hardness

The hardness of each sample was measured by Shore A Durometer (GIBITRE Instrument, Italy) as per ASTM D 2240-05 test method. The average of four observations has been taken

3.4.2 Tensile and Tear

Tensile (dumbbell shaped) and tear (angle shaped) specimen were punched out from the molded sheets by Hollow Die Punch (CEAST, Italy).The test were carried out in a Universal Testing Machine (ZwickRoell Z010, Germany) at a cross head speed of 500mm/min at 25±2°C .Tensile and tear tests were carried

out as per the ASTM D 412-98 and ASTM D 624-00 respectively. Results of tensile and tear tests for each sample was noted down and the average of five repeated observations was taken for the study. The standard deviation for modulus (M300%), tensile strength (T.S), elongation at break(EB) and tear strength are±0.3,±0.7,±0.8 and ±1.5 units respectively.

3.4.3 Abrasion Index

The samples were prepared using a three piece-sixteen cavity mold and the testing was carried out in DIN abrader as per ISO 4649 (ASTM D5963-04)

3.4.4 Heat Build-up

For this test a simple three-piece, sixteen cavity mold was used for making cylindrical rubber specimens, having diameter of 17.8mm and height 25 mm according to ASTM D 623-93 for Goodrich Flexometer Tester. Samples were cured at 160°C for 30minutes. The samples were preheated for 25 minutes to reach thermal equilibrium of 50°C.The test was carried out for 25 minutes by cyclic hammering at 1800 rpm with each stroke length of 4.45 mm. The average of three samples was taken. The error was found to be ±0.20°C

3.5 DMA

Dynamic Mechanical Analysis of the samples was performed by using a Dynamic Mechanical Analyzer-DMA 4000, (Metravib, France). Liquid nitrogen was used as the coolant for low temperature measurements.

Strain sweep was done in tension mode at variable temperatures from 40^0C to 80^0C in 3 steps & at constant frequency of 1Hz with the strain ranging from $1x10^{-4}$ to $1x10^{-1}$.

Temperature sweep was done in tension mode at constant strain 0.25% and frequency 10 Hz. The temperature range is from -35^0C to $+80^0$C.

Frequency sweep was done in tension mode in 13 steps with temperature starting from -30^0C to $+40^0$C centigrade and static strain 0.001%. The samples were tested at frequencies varying from 1Hz to 50Hz at 0.01% dynamic strain at different constant temperature between -30^0C to 40^0C.

The storage modulus (E'), loss modulus (E") and tanδ values were measured as a function of temperature under the tension mode. Those values were taken into account, to have information about Tanδ (as damping).WLF master curves were plotted using the C_1, $\&C_2$ values obtained from DMA.

3.6 LFT measurements

Only the sliding behaviour of single tread blocks was considered in this study. The tread block with the simplest shape, which constitutes the elementary unit of any tread pattern, has no sipes and a rectangular cross-section. Such blocks give a close approach to realistic tread patterns. It employs a macroscopic approach to maintain simplicity and efficiency of its application. Friction is a dissipative process. It results in heat generation and consequently, in heating of the contact surface. In case of rubber friction, the major part of energy dissipation results from periodic deformations of the rubber in layers adjacent to the contact surface.

Through the LFT results we obtain the coefficient of friction which results from the adhesive friction $F_{ADHESION}$, hysteresis friction $F_{HYSTERESIS}$ and friction due to edge effect $F_{SHAPE-FACTOR}$. The former two phenomenon are mainly from the elastomer characteristics and the edge effect is driven by geometry of the tread block and shear stiffness of tread-tire carcass interaction. Because of pressure concentrations, the front edges of the single blocks tend to stick at the contact surface and to curl up.

In this study, the dry and wet condition is considered for determining the frictional coefficient by the LFT measurements. In dry inter-facial condition, both adhesion and hysteresis components contribute towards the frictional coefficient along with the edge effect which is inevitable, whereas in wet inter-facial condition, the adhesion component of the frictional coefficient is inconsequential.

The number of runs for each set of test series is carried out for 3 cycles for dry condition and for 5 cycles for wet condition. The sliding distance is limited to 300mm on the LFT substrate. The mean value of friction coefficient is recorded for analysis. The frictional coefficient is calculated for 3 different sliding velocities to 4 increasing normal pressure. The different sliding velocities selected for the test are to simulate the real rolling friction of tires at normal-high speeds and the sliding friction during the wheel lock condition while braking at very high speeds. The different sliding velocities selected are 10mm/s, 100mm/s and 1000mm/s. The low

magnitude of sliding velocities relates more over static friction phenomenon and the high magnitude determines the dynamic friction behaviour of the tread block.

The different pressure applied on the rubber block simulates the significance of unladed vehicle to a loaded vehicle. The magnitude of pressure applied on the rubber block ranges through 0.25 MPa, 0.50 MPa, 1.50 MPa and 2.0 MPa.

Chapter 4

Results and Discussions

4.1 Rheological Properties

Cure study of the samples are carried out at 160°C for 30 minutes. A typical cure curve can be analyzed into three regions of scorch delay, crosslinking and reversion periods. The first region is the scorch delay period or induction period, in
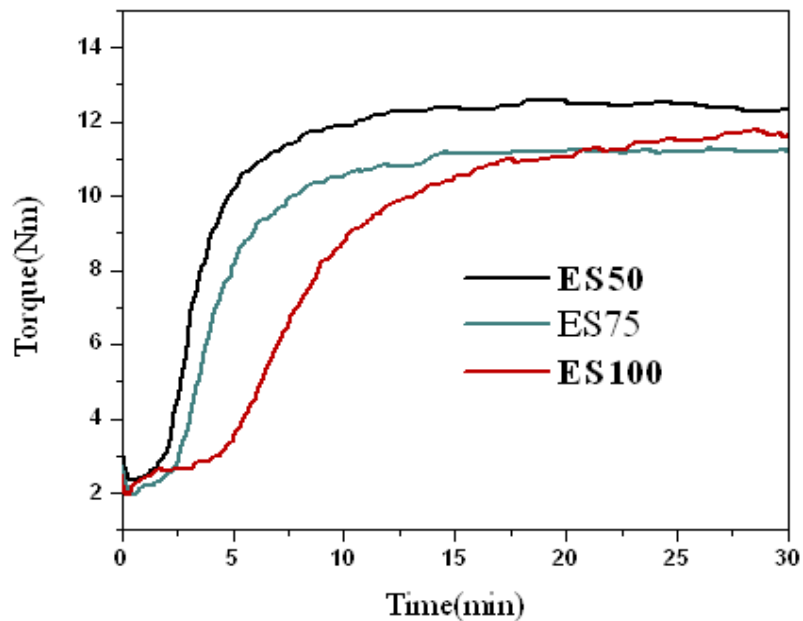
Figure 19: Rheo curve from α technologies MDR 2000

which most of the accelerator chemistry takes place. The second period is the crosslinking period, in which the initial network structures are formed and the intermediate accelerators are consumed. The final stage is the over cure or reversion period. In figure 19 T_{S2} and T_{C90} increase with increase in silica content this shows that ES100 has better scorch safety but higher cure time. Table 3 shows the cure characteristics of the samples.

Cure characteristics at 160° C for 30 minutes					
Compound	ML (lb-in)	Mh (lb-in)	TS2	Tc50	Tc90
E50S50-50Si-50C	2.23	12.59	2.42	3.35	7.47
E50S50-75Si-25C	1.95	11.27	3.02	4.07	8.7
E50S50-100Si-0C	1.95	11.62	5.38	7.58	15.98

Table 3: Shows the cure characteristics of samples

Silica has been used as an important reinforcing agent in rubber compounds together with carbon black.[1-4] Silica has enormous hydroxyl group on its surface, which resu lts in strong filler-filler interactions and adsorption of polar materials by hydrogen bonds[5]. Since the intermolecular hydrogen bonds between hydroxyl groups on the surface of silica are very strong, it can aggregate tightly. For silica filled rubber compounds with an accelerated sulfur cure system, the curatives are adsorbed on the surface which results in slow cure characteristics. Since the silica surface is acidic, it forms especially strong hydrogen bond with basic materials. CBS (N-cyclohexylbenzothiazole sulfenamide) is used as the cure accelerator system for all the formulations, since they have basic functional groups, such as amide (=NH), they are most readily adsorbed on the silica surface[1]. The adsorption of curatives by silica results in delay of the scorch time, reduction of the Δtorque and in turn increase the cure time of silica filled rubber compound. The silane coupling agent reacts with silanol on the surface of silica to form a siloxane bond. Silane coupling agent TESPT (bis-[3(-triethoxysilyl)-propyl]-tetrasulfide) is used in this system to improve the filler dispersion and to prevent adsorption of the curatives on the silica surface[1]. The silane molecule bonded to the silica surface reacts with the rubber to form crosslinks between silica and the polymer.

4.2 Physical Properties

4.2.1 Hardness

Hardness of the three samples is studied and shows that when the silica content increases with decreasing carbon black, the hardness decreases gradually. Compared to carbon black, a higher amount of silica is needed in order to achieve the same hardness level. This is thought to be due to the decrease in crosslink density when high silica loading is used. Table 4 shows the Shore a hardness values of the samples. ES100 has the lowest hardness than ES75 & ES50.

Compound	Shore A
ES50	63
ES75	59
ES100	55

Table 4: Hardness of the samples in Shore A units

The explanation is given as the adsorption of zinc complex on the silica surface, thus lowering the sulfur vulcanization efficiency.

4.2.2 Tensile & 4.2.3 Tear strength

Increase in silica content cause a continuous decrease in modulus. ES100 has low modulus than ES75 & ES50 at 100%, 200% and 300%. Tensile strength and elongation at break values do not follow a clear trend; this is also observed by several
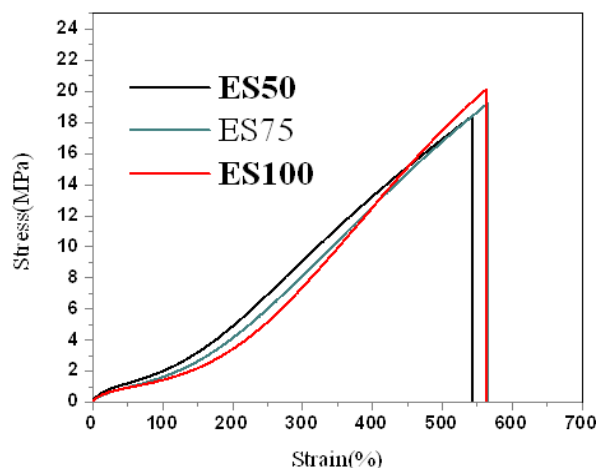
Figure 20: Tensile properties of samples

researchers. Tensile strength more or less remains same for all the compound design. Table 5 shows the tensile properties of the samples.

Compound	M 100 (MPa)	M200 (MPa)	M300 (MPa)	Tensile (MPa)	E.B %	Tear N/mm
ES50	2.02	5.03	9.34	18.50	540.00	50.36
ES75	1.65	4.15	8.20	19.25	566.00	49.12
ES100	1.40	3.40	7.38	20.16	562.00	49..96

Table 5: Tensile strength properties of the samples

4.2.4 Resistance to Abrasion

Abrasion/wear resistance is a significant measurement for any passenger car tire. Generally carbon black formulations are very resistant to wear loss measured with the test method adopted. In practice, the additional cycling loading induces hysteresis phenomenon in the tread block. This shows a higher wear rate in carbon black formulations than the lab measurements.

Compound	Avg. wt loss (mg)	Abrasion loss (mm3)	Sp. Gravity	ARI (%)
ES5050	179.9	113.55	1.198	130.3
ES75	223.3	140.24	1.204	105.5
ES100	348.9	216.05	1.221	68.5

Table 6: Abrasion resistance of the samples from DIN Abrader

In general, for silica compounds, the abrasion index are about 20 - 40% lower than carbon black –silica dual phase formulations. It is well seen from the Table 6, that the abrasion resistance index (ARI%) is constantly decreasing with increasing the silica filer loading.

4.2.5 Heat Buildup

Filler networking is the main factor governing the heat build-up (hysteresis) of the compound. Stable filler network or better filler-polymer interaction

cause reduced hysteresis. ES50 has very high hysteresis loss compared to other two samples. ES100 has the least hysteresis loss. The heat build-up results of the samples are summaries in table 7.

Temperature in °C

Sample	Initial sample temperature	Base Final Temperature	Centre Final Temperature	Sample base heat build-up	Sample center heat build-up
ES50	70	107.2	155.0	37.2	47.8
ES75	70	105.0	153.3	35.0	48.3
ES100	70	105.0	152.2	35.0	47.2

Table 7: Heat build-up results of the samples from Goodrich flexometer

The loss due to hysteresis is seen least for ES100 compared to ES75 and ES50. Figure 21 shows the hysteresis loop of the samples. This is synchronizing with the heat build-up results. Table 8 shows the energy dissipation values of the samples for 10 cycles. The magnitude of the loss is less for ES100 compound, and the Δ Energy loss $\sim$ Zero after 5 cycles. This
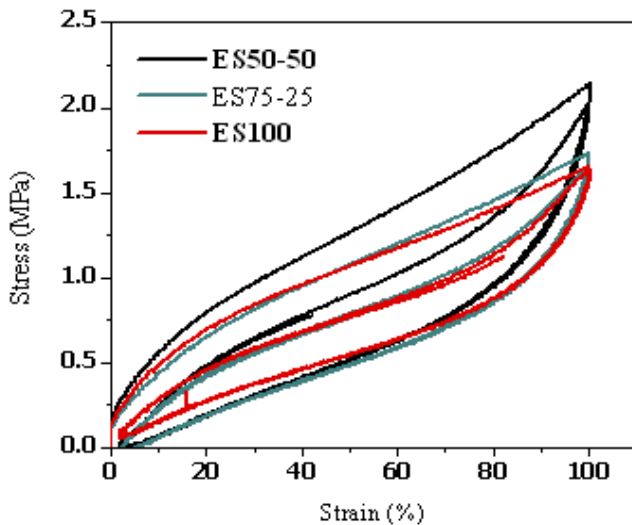
Figure 21: Hysteresis loop of the samples

Samples	ES50-50	ES75-25	ES100
Cycles	Energy	(Joule)	
1	0.231	0.175	0.153
2	0.114	0.091	0.071
3	0.106	0.083	0.065
4	0.102	0.079	0.062
5	0.101	0.078	0.061
6	0.099	0.077	0.058
7	0.098	0.076	0.058
8	0.097	0.076	0.058
9	0.096	0.074	0.057
10	0.095	0.074	0.057

Table 8: Energy loss in hysteresis of the samples

shows the influence of chemical linkages of the silica filler to the SBR elastomer matrix. The physical interaction of the carbon black – elastomer is rupturing during the deformation cycles.

4.3 DMA Results

4.3.1 Strain sweep

Comparative quantitative assessments of filler network deformations of three samples are found out through the strain sweep at 60 ºC within the strain range of 0.01% to 10.0%; illustrated in fig 22. Mechanical stability of the samples can be inferred from strain sweep measurements; i.e. higher the Δ E' (Payne effect) poor the mechanical stability. ES100 is found out to have a lower delta E' compared to ES75 & ES100. It is known that the filler aggregates in the polymer matrix have a tendency to associate to agglomerates, especially at high loading, leading to chain-like filler structures or clusters. These are generally termed secondary structure or, in some cases, filler network.[8-10]. It has been reported that the modulus of the unfilled compound does not change significantly upon increasing strain amplitude over the range of double strain amplitude tested; it decreases for the filled rubber, showing a typical non-linear behavior. This phenomenon was observed in 1950 by Warring[11] and later it was studied extensively by Payne after whom the effect is often named[9, 12]. This effect is exponentially
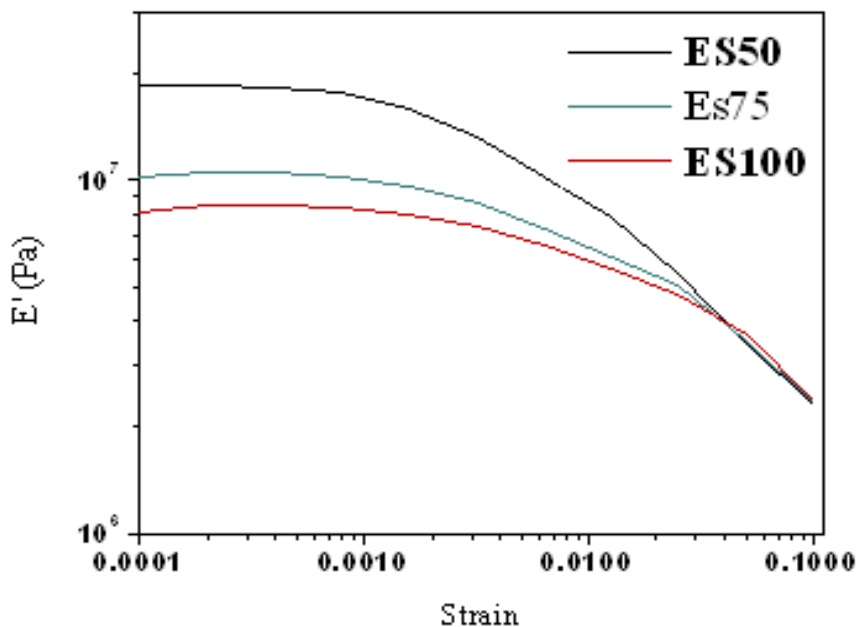
Figure 22: Strain sweep of the samples

increased by increasing filler loading. The decrease in elastic modulus upon increasing strain amplitude was attributed by Payne to "the structure of the carbon black, and may be visualized as filler-filler linkages of physical nature which are broken down by straining".[13] This structure was further clarified by Medalia as that "inter-aggregate association by physical forces, not the structure" or aggregate bulkiness" as generally termed in the rubber industry.[10] It is understandable that the rubber trapped or caged   in the filler network or agglomerates would be at least partially "dead", losing its identity as an elastomer and behaving as filler in terms of stress-strain properties.   Therefore, the effective volume of the polymer bearing the stresses imposed upon the sample is reduced by filler networking, resulting in increased modulus which is governed primarily by   the filler concentration.

In   other   words,   filler-polymer interaction can be inferred from delta E' value   or   tan δ peak. Lower $\Delta E'$ (lower tan δ peak) better will be the filler polymer interaction and subsequently lower rolling resistance. Figure 23 shows the tan delta plot of the samples are different strain levels. With carbon black, silica and carbon-silica dual phase fillers, if the filler network cannot be broken down, the elastic modulus
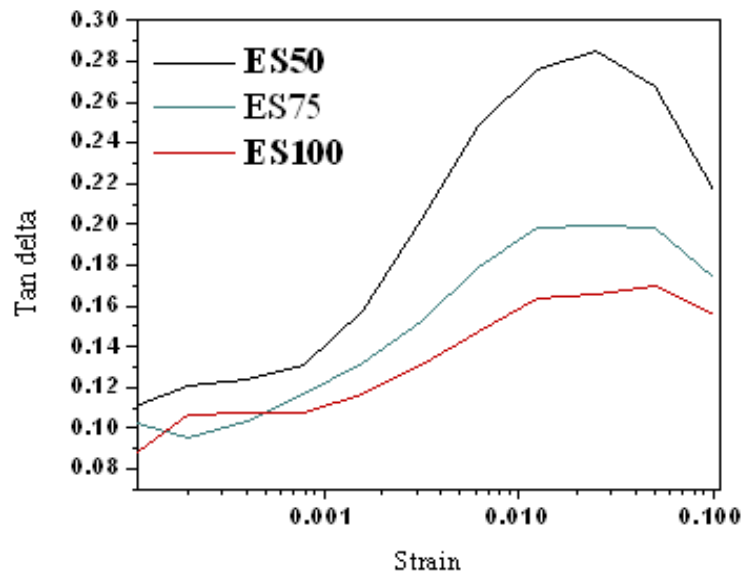
Figure 23: Tan δ plot of the samples at different strain levels

would increase substantially due to the rubber trapped in the network. The breakdown and reformation of the filler network, which may release the trapped rubber for energy dissipation, would cause an additional energy dissipation process, imparting higher hysteresis to the- filled rubber. Compared to carbon black, silica assisted with TESPT coupling agent showed less tendency to form a filler network; giving lower hysteresis at high temperature and higher hysteresis at low temperature.

Strain sweep-kinetics
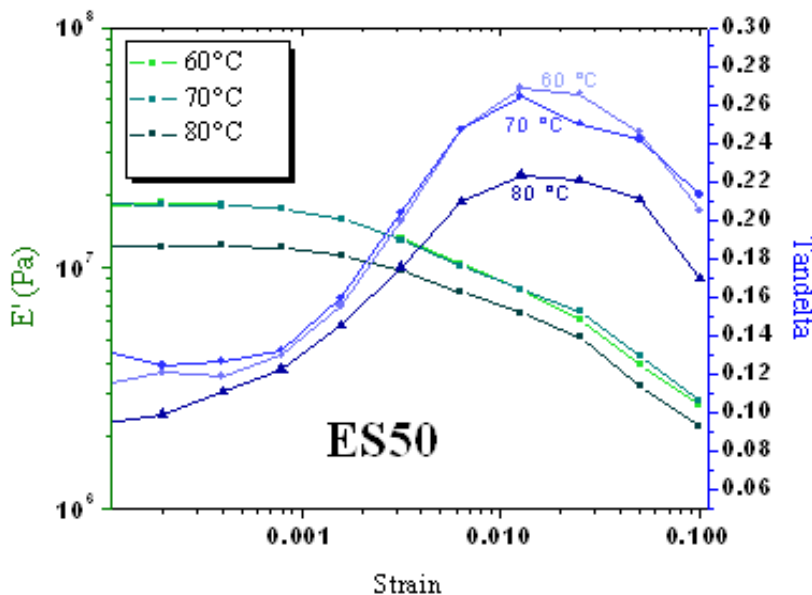
Figure 24: Strain sweep of the ES 50 sample at different temperatures

From the above tests, ES75 shows the intermediate results which are more shifted towards ES100 properties. So for further analysis ES50 and ES100 were considered. As seen in figure 24 & 25, the storage modulus at low amplitudes E'_0 decreases with temperature, whereas the storage modulus at high amplitudes E'_∞ remains more or less constant. Similarly, in figure 24 & 25 the loss factor (tanδ) shows temperature dependence for low strain which increases at larger strain

amplitudes. The peaks in the tanδ vs. strain amplitude correspond to the strains where the strongest decrease in storage modulus is observed.

The dependence of the Payne effect in storage modulus for different silica filler formulations is more for higher silica loading. And at high strain levels, Payne effect is less pronounced with increase in the filler loading.[14]

Figure 25: Strain sweep of the ES 100 sample at different temperatures

ES50 is having a poor fit & lower activation energy which is required to disintegrate the filler network & ES100 is having a better fit and higher (activation) energy for which it is required to disintegrate the filler network structure. Figure 26 shows the curve fit of Payne effect of ES50 & ES100 samples.
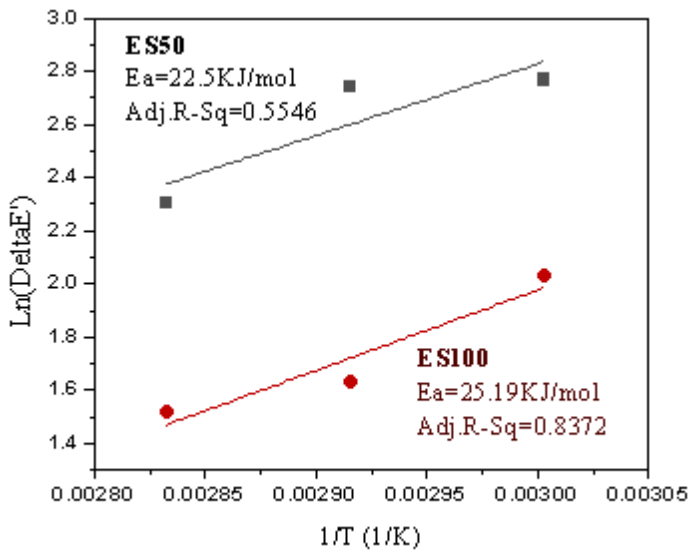
Figure 26: Payne effect plots for ES50 and ES100 compounds

4.3.2 Temperature sweep

Temperature sweep is carried out for ES100 and ES50 samples and ES100 sample shows higher tan δ values at low temperature regime. It is well known that hysteresis of tread composites, characterized by tan δ, at 60°C temperature, is a key parameter which shows a good correlation with the rolling resistance of tires. Details of the tan δ curve are listed in table 9. On the other hand, it has been widely accepted that the hysteresis at lower temperatures (-10°C to +20°C), related to the high-frequency nature of the dynamic strain involved in the skid process, is of importance.

Sample	Tg°C	Tan δ @ 0°C	Tan δ @ 60°C
ES50	-15.2	0.395	0.208
ES100	-12.8	0.528	0.147

Table 9: T_g, WSR, RR values of ES50 and ES100 samples from temperature sweep
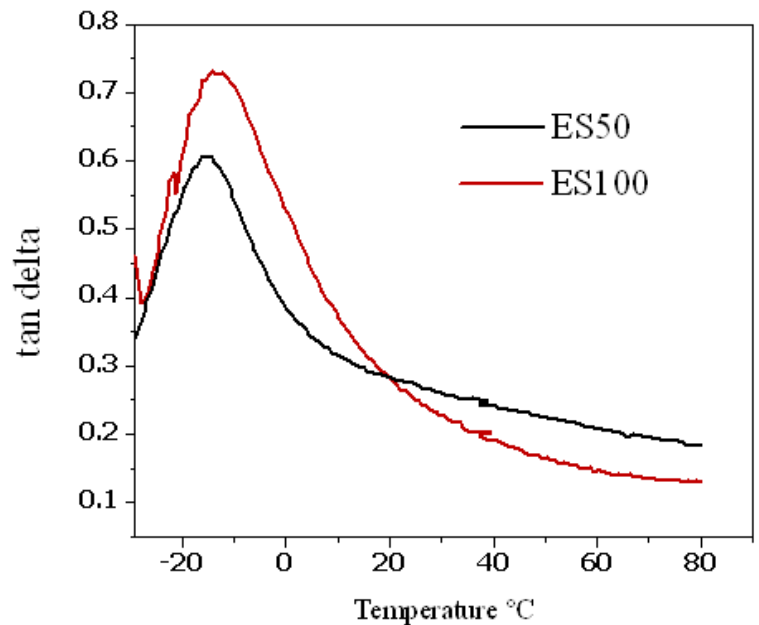
Figure 27: Temperature sweep tanδ curves of ES50 and ES100 samples

The temperature dependence of tan δ & T_g of ES50 and ES100 tread samples at constant frequency are shown in figure 27. Higher hysteresis at lower temperature (0°C) will be favorable for wet-skid resistance[15]. Highly loaded silica compound shows low RR and high wet traction characteristics.

4.3.3 Frequency sweep

Frequency sweep for samples ES50 and ES100 are carried out at temperature range of -40 ℃ to 40 ℃ through 1 to 50 Hz. Figure 28 shows the frequency sweep curve for ES50 sample from Metravib 4000.
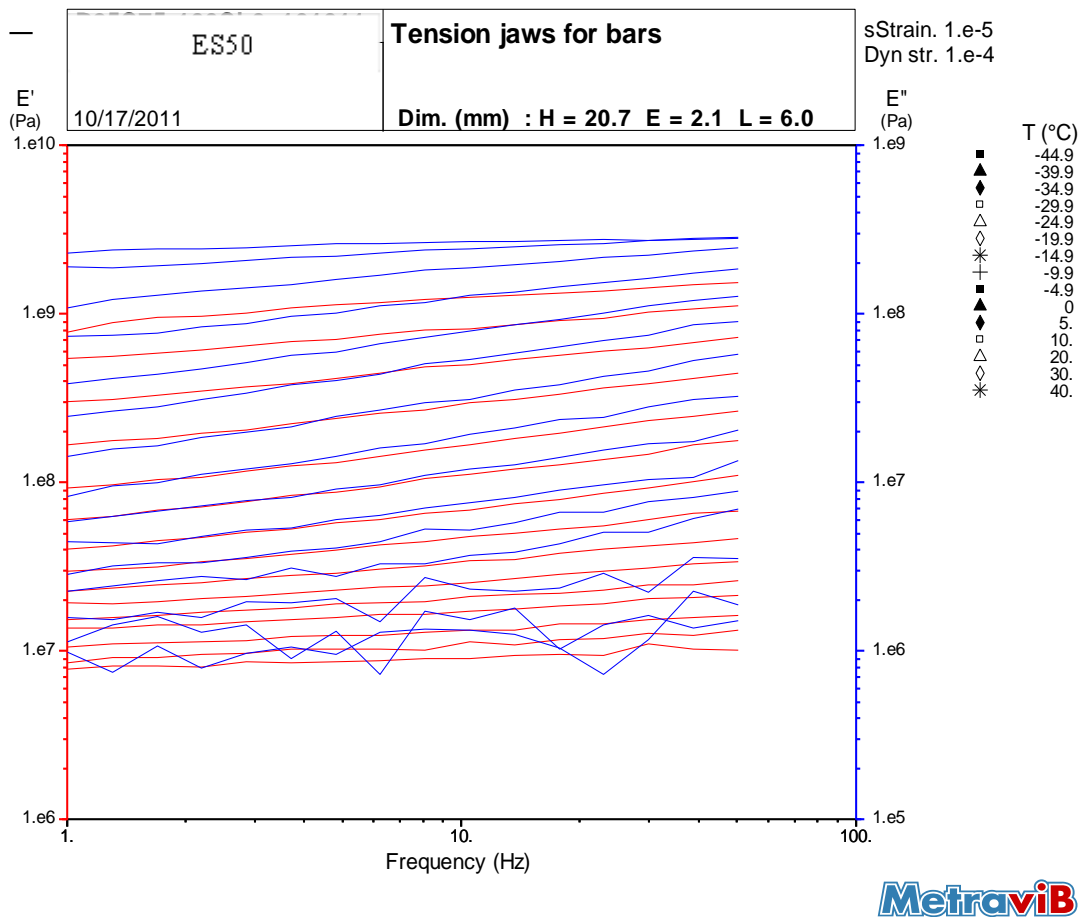
Figure 28: Frequency sweep curve for ES50 sample from 1Hz to 50Hz

Master curve by Frequency-Temperature Superposition technique:

Using WLF transform, the high frequency behaviour is analyzed. According to the frequency-temperature-superposition principle (FTS), frequency influence can be replaced by temperature influence, where cold rubber equals high frequency treatment and causes a glassy state with high stiffness,

whereas a warm elastomer dominated by rubber matrix/ filler is connected to low frequencies. Indeed, by applying various frequencies at discrete temperatures on the sample, we get a bunch of branches for the moduli that can be constructed to a master curve for the whole frequency range over several decades by shifting the branches horizontally in order to form a continuous curve. The FTS is not valid anymore for filled elastomers in this temperature range, because the filler-filler bond instead of the polymer matrix then dominates the viscoelastic behaviour[22]. In addition to horizontal shifting (*At*) of storage modulus (E') and loss modulus (E''), vertical shifting (*Bt*) is also required for the filled compounds to compensate it.

Horizontal Shift:

Frequency – Temperature superposition is basically a frequency sweep at different temperatures for a specified dynamic strain. To produce master curves for these filler reinforced compounds, first a horizontal shift is done along the frequency axis. The WLF equation has been used to calculate the horizontal shift factor *At* according to equation (2). T_g+50 ºC and the corresponding universal constants were chosen as reference temperature and C_1 and C_2, respectively. The T_g values for different compounds filled with different amount of filler were almost the same: -14.0±1ºC. The master curve is not smooth and some overlapping of the curves at the low frequency region occurs. The physical origin of this overlapping is the superposition of two relaxation processes, the one of the polymer matrix and that of the filler network[16]. Figure 29 shows the master curve of ES50 sample without vertical shifting. Stacking of the curves, one over the other is seen in the plot shifted to lower frequency and higher frequency region. These gaps are compensated by introducing the vertical shifting procedure.
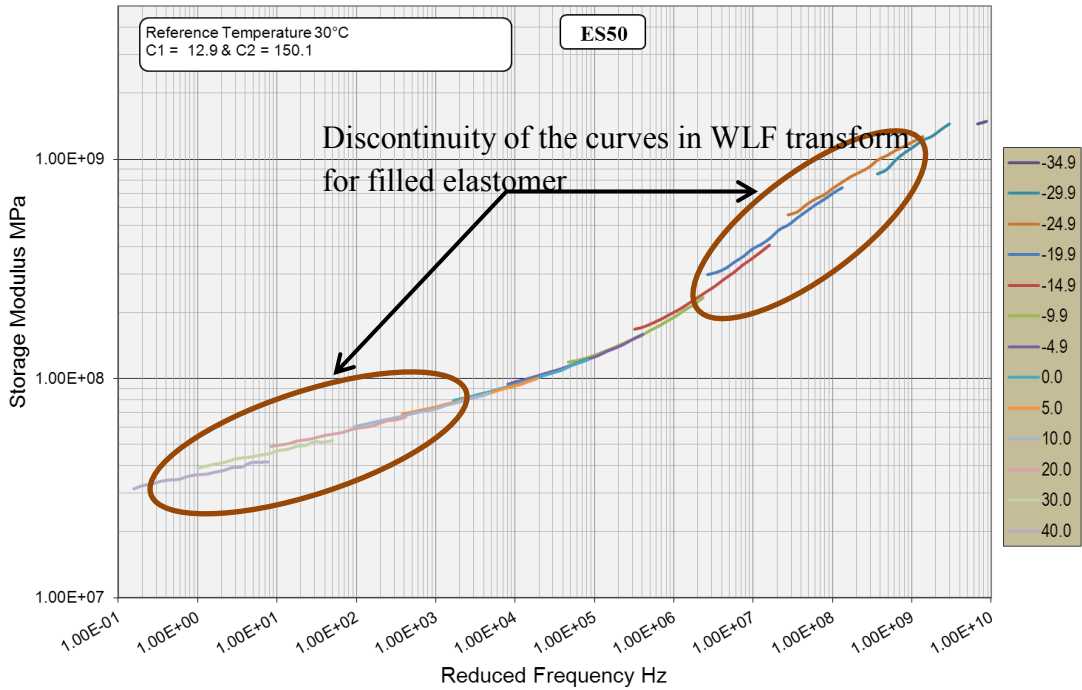
Figure 29: WLF master curve of ES50 sample without vertical shift

Vertical shift:
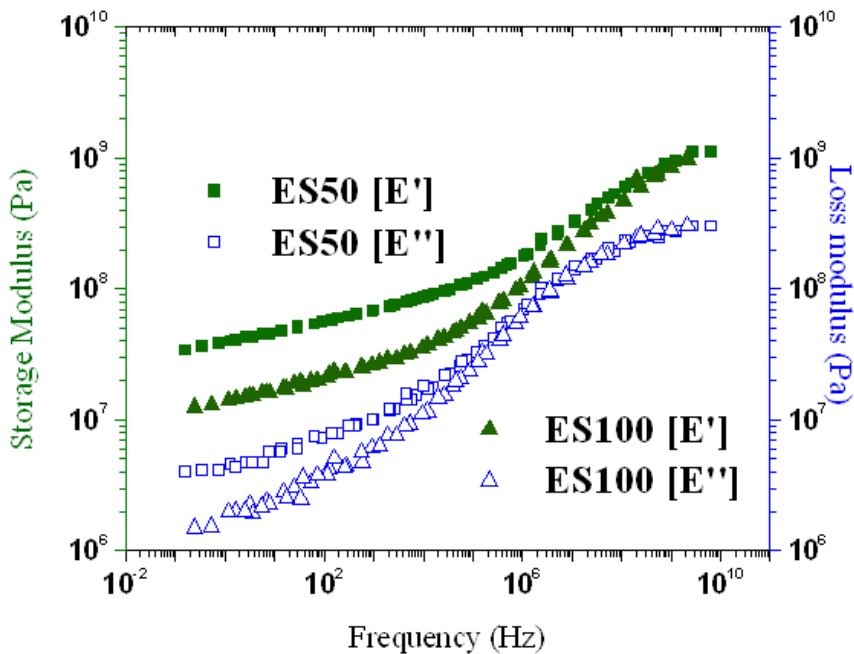
Figure 30: Master curves of ES50 & ES100 with vertical shift

In order to obtain a proper master curve, vertical shifts are necessary to be applied. For unfilled, non-reinforced polymers the vertical shift is commonly applied to account for the density-change of the polymers with

temperature. Vertical shift is mainly intended to include the influence of filler network structure, which in turn is a thermally activated process. However, because the filler network greatly overrules these polymer effects, it is necessary to include the vertical shift for the generation of mater curves. The vertical shifting was done numerically through Origin Pro and MS Excel programs. During vertical shifting, the curve for the reference temperature were kept unchanged and the other isothermals shifted vertically by respective vertical shift factors *Bt*. The reference curve at 30°C is selected for the master curve generation for ES50 and ES100 samples. A nice smooth curve is obtained after including the vertical shift factors. Figure 30 shows the master curve of E' & E'' for ES50 and ES100 samples.

It has been stated before that in the high frequency (low temperature) region, unreinforced gum rubber performs best in terms of WSR. In this region, the transition zone, the polymer chains themselves are responsible for the energy dissipation[17]. By introduction of fillers, the fraction of free polymer chains decreases due to the fact that the polymers near to the filler surface are partly immobilized and act as filler rather than polymer: the occluded rubber concept and/or the concept of a glassy shell around the filler particle[18-21].

The trend of Horizontal (*At*) & Vertical (*Bt*) shift factors

Figure 31: Shift factors *At* & *Bt* of ES50
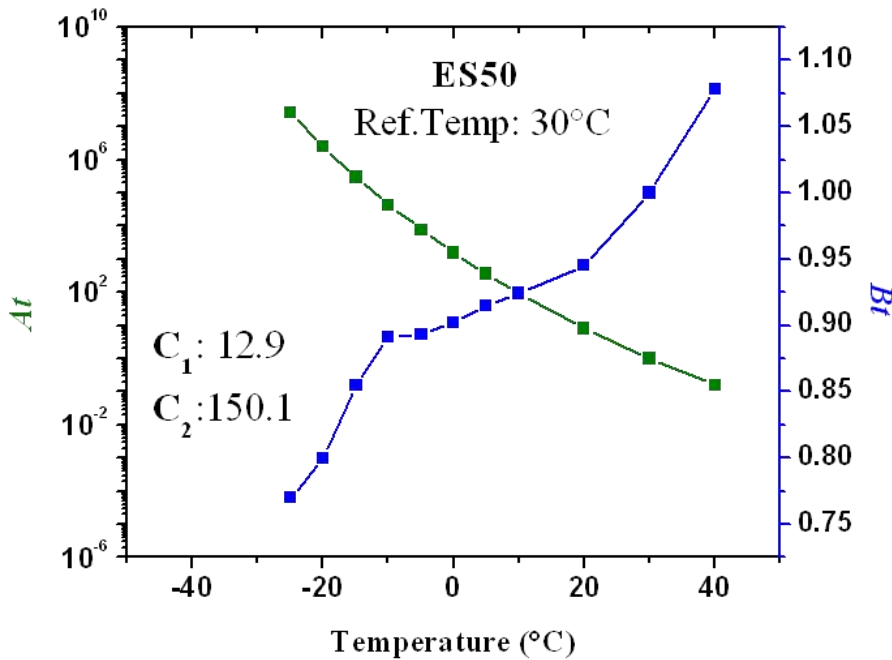
The shift factor *At* shows a good trend. Vertical shift factor *Bt* is slighty deviating for ES100 sample. It is mostly due to the high amount of filler, which is responsible for filler networks.

Figure 31 & 32 shows the shift factor trend for ES50 and ES100 samples.
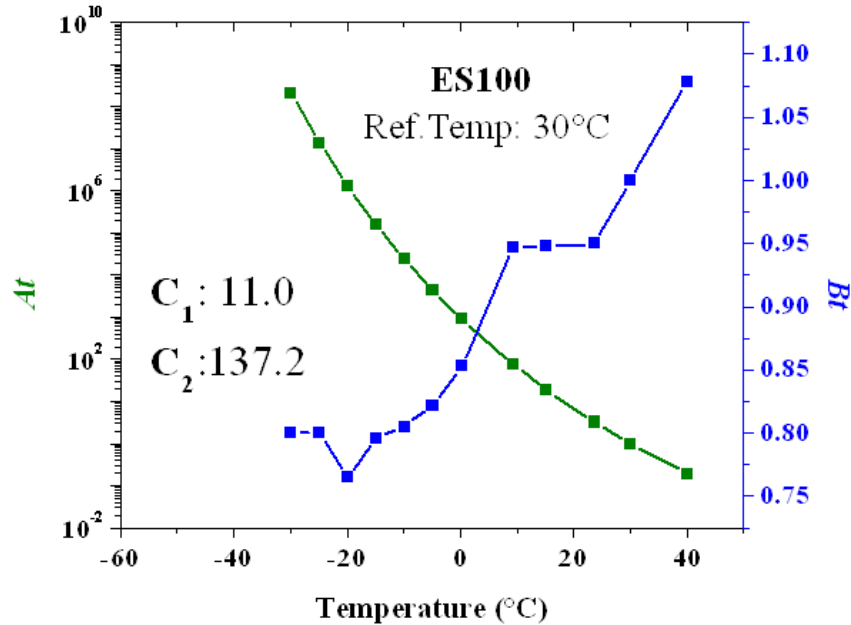
Figure 32: Shift factors *At* & *Bt* of ES100

4.3.4 WLF Master curve of **tan δ**

ES100 is having a higher tan δ values at the WSR regime of frequencies 0.1MHz to 100MHz. Tan δ values are calculated from the E'' and E' magnitudes after including both *At & Bt* shift factors. Then those values are plotted against the reduced logarithmic frequency. Figure 33 shows the tan δ curve of ES50 and ES100 samples.
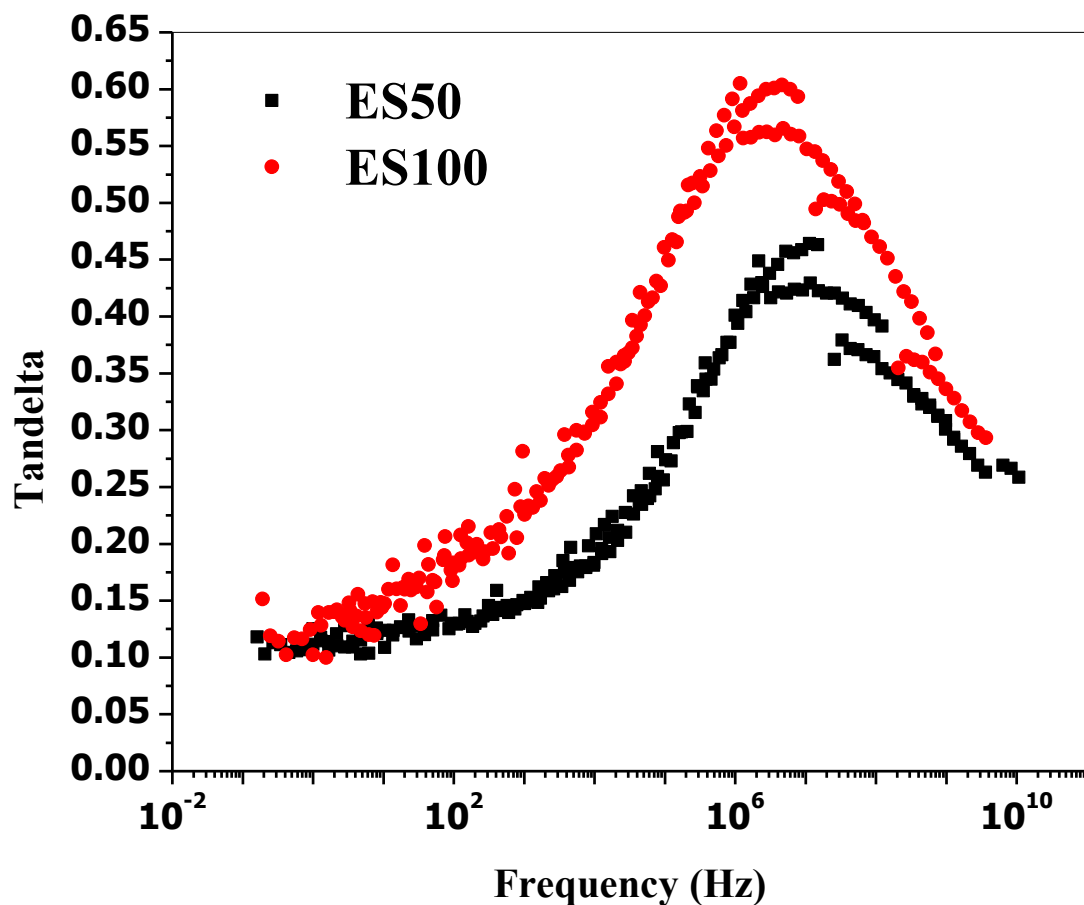
Figure 33: Tan δ master curve of ES50 & ES100

The tan δ values are seen enhanced for ES100 sample having more amount of silica.

Frequency sweep and temperature sweep equivalence
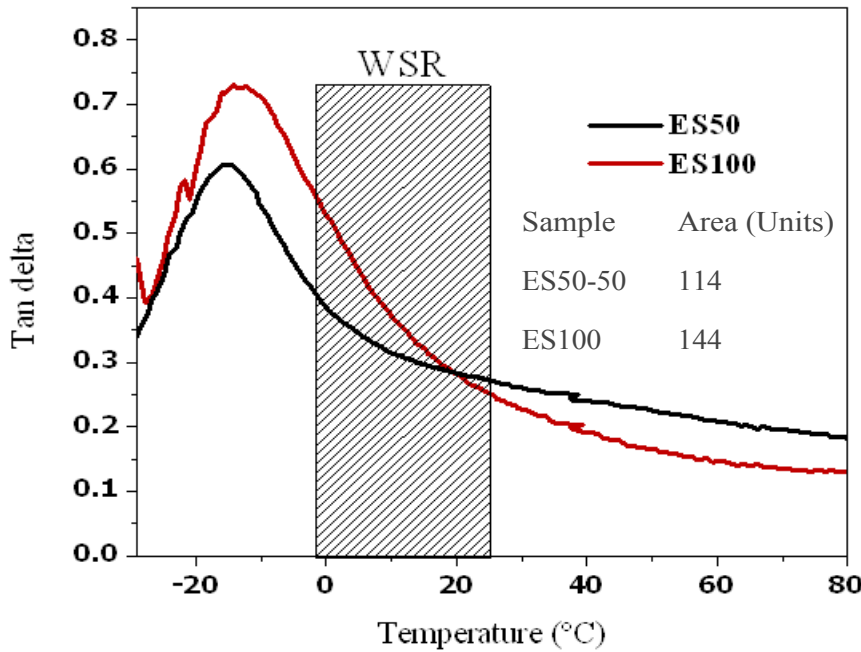
Figure 34: Area of tan δ in Tsweep for ES50 & ES100

For WSR or RR, tan δ is considered as the key input for the prediction of real performance. In reality, the range of tan δ values at the vicinities of the WSR and RR region gives better insight for real time prediction. Here in this study, the tan δ curve at temperatures from -10°C to +20°C are used & similarly the tan δ curve at frequencies 0.1MHz to 100MHz are considered for the wet skid performance of the tread compound. Figure 34 & 35 shows the tan δ equivalence in frequency sweep and temperature sweep.
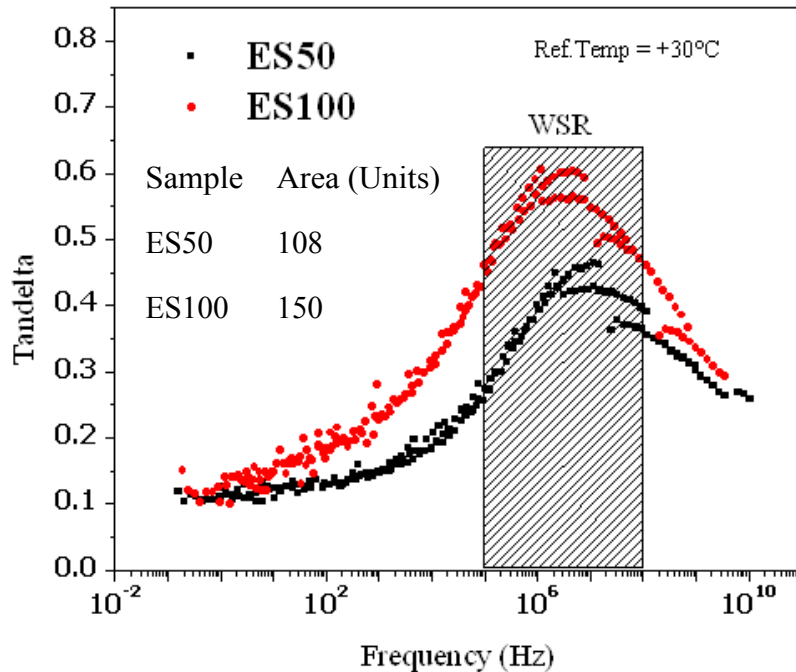
Figure 35: Area of tan δ in WLF for ES50 & ES100

4.4 LFT results

Experimental investigations of the sliding behaviour of rubber blocks are performed at Linear Friction Tester (LFT). LFT is capable of testing the samples at various slip velocities. The extreme boundary conditions such as low slip velocity to very high slip velocity could give the real time tire rolling friction and sliding friction. Therefore the results from these test conditions are well suited for the study.
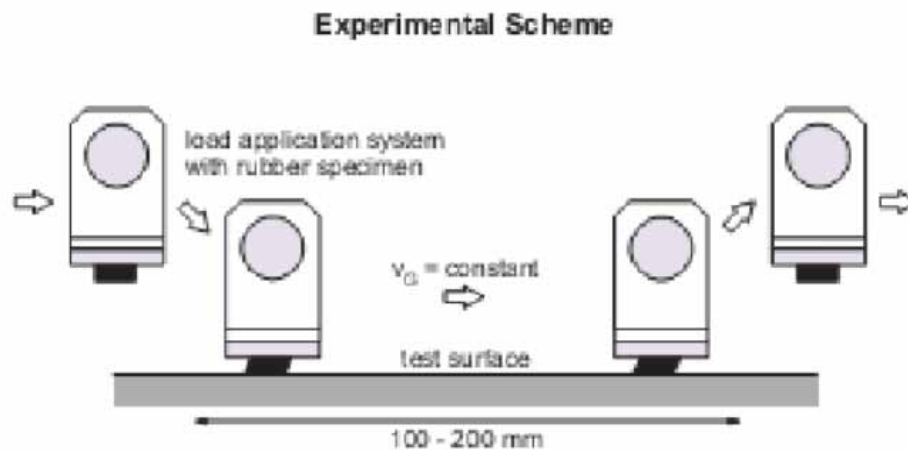
Figure 36: Mechanism of sliding the specimen over the substrate

Figure 36 shows the mechanism of sliding the specimen over the substrate. Coefficient of friction is discussed further in detail with varying the normal load and sliding velocity. Results of the frictional coefficients are plotted with respect to their sliding velocities and normal pressure.

4.4.1 Dry condition

In dry condition, the adhesion component and hysteresis component of friction plays for grip performances. The samples ES50 and ES100 were performed the LFT measurements for frictional coefficients in dry condition at different normal pressure and sliding velocities. It is clear that ES 100 showed better friction coefficients than ES50 sample. It is also observed that

the frictional coefficient increases to a threshold and then reverses as the sliding velocity increases at all levels of normal pressure used for the analysis.
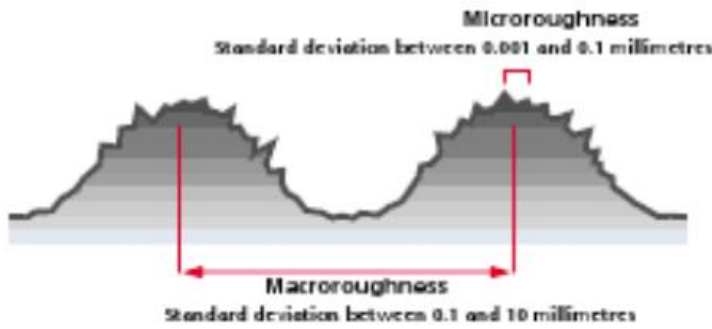
Figure 37: Macro and Micro roughness on dry surface

Figure 37 shows the magnified view of the dry substrate with macro and micro roughness profile. At extreme normal pressure, the rate of change of friction coefficient is marginal as there plays cutting and chipping phenomenon of the samples during the test, so there is a decrease in the friction coefficient values even at lower pressure. Figure 38 shows the dry friction coefficient ES50 at various normal pressure & sliding velocities.
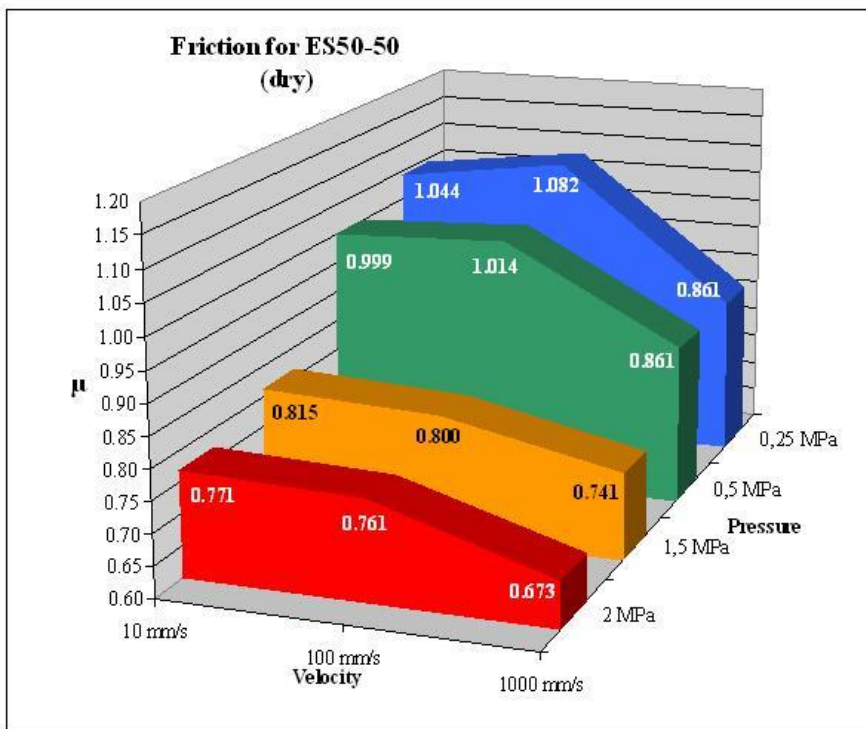
Figure 38: Dry friction coefficient for ES50 sample

Sample ES50 shows a distinct parabolic trend of friction coefficient at lower normal loads from 10mm/s to 1000mm/s sliding velocities.

At extreme conditions, the trend is deviating from the previous normal pressure. The dual phase silica and carbon black filler is less beneficial for skid performance. Δµ between 0.5MPa and 1.5MPa is high enough to risk during dry grip performance. Increasing the silica loading visibly enhances the dry friction coefficient at all the conditions. Figure 39 shows the dry friction coefficient ES100 at various normal pressure & sliding velocities.
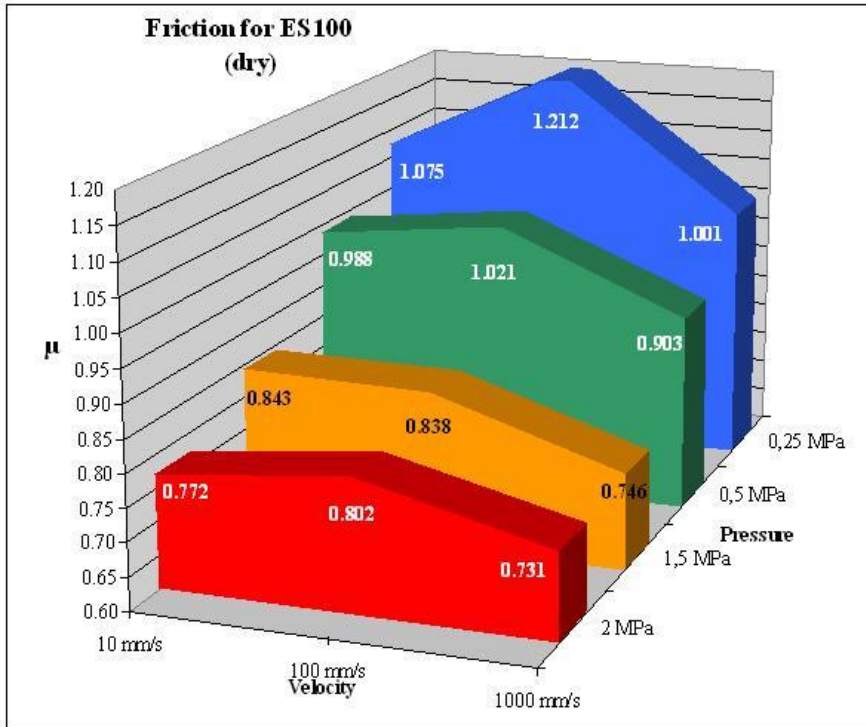
Figure 39: Dry friction coefficient for ES100 sample

Sample ES100 without any carbon black shows better magnitudes of friction coefficients. At lower normal pressure (0.25 MPa and 0.5MPa) shows good parabolic trend of friction coefficient compared to ES50. At extreme conditions, the trend is deviating which is due to chipping and cutting of edges of the test specimen. So at dry condition, ES100 performs better than ES50 compound. This ensures that increasing the amount of silica in the compound design enhances the dry grip performances.

4.4.2 Wet condition

In wet condition, the adhesion component of friction is marginal and predominantly the hysteresis component plays for predicting the grip performance. Figure 40 shows the magnified view of the wet substrate with macro and micro roughness profile. The compound ES50 reflects a very high dip in the frictional values at sliding velocity 1000mm/s for all normal pressures applied.
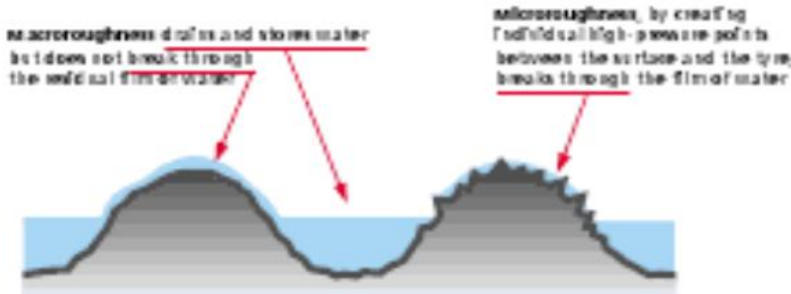
Figure 40: Macro and Micro roughness on wet surface

Figure 41 & 42 shows the wet friction coefficient of ES50 & ES100 at various normal pressure & sliding velocities. At extreme conditions of loading (1.5MPa and 2.0 MPa) and sliding velocities (1000mm/s) wet friction measurements are not precise. Only with the hysteresis component and the absence of adhesion friction the specimen is not experiencing sufficient relaxation time to overcome these snags. Increasing the silica content shows better wet friction coefficient at higher sliding velocities.
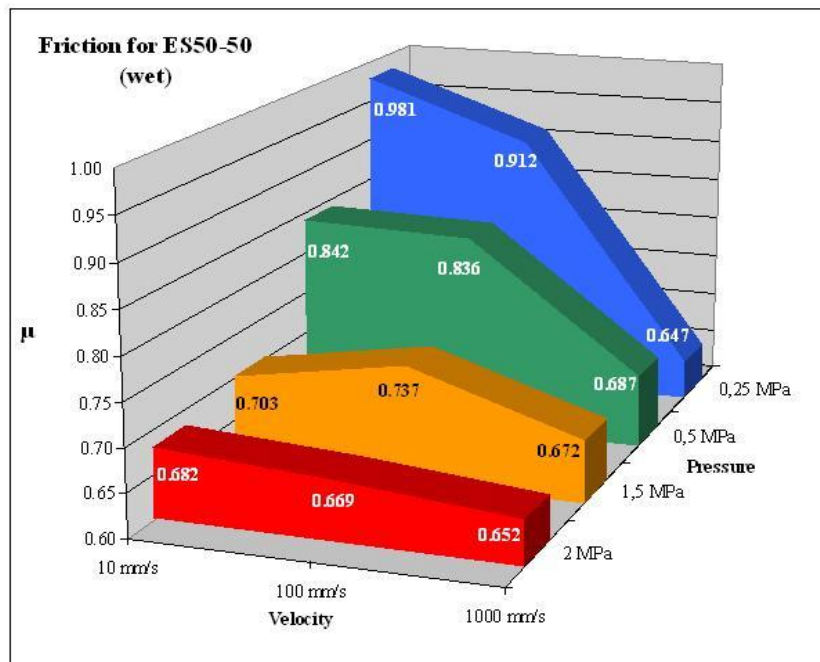
Figure 41: Wet friction coefficient for ES50 sample

At lower loads (0.25MPa and 0.5MPa) and sliding velocities, ES100 shows

better wet grip performance than ES50 and wet friction coefficient follows the parabolic trend from 10mm/s to 1000mm/s sliding velocities. Further increasing the load suddenly decreases the wet friction
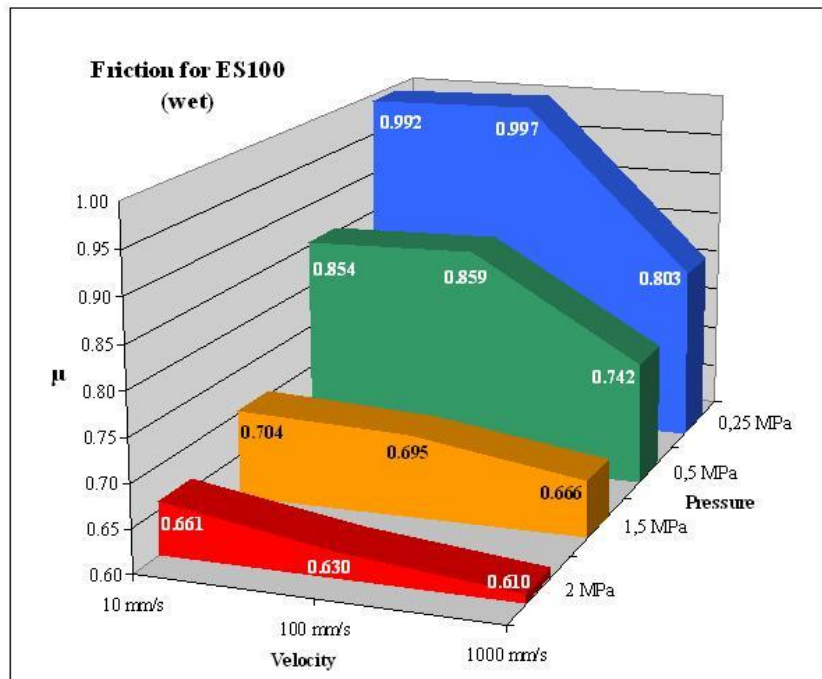
Figure 42: Wet friction coefficient for ES100 sample

which is due to the insufficient relaxation time for the test sample used.

Wet friction as a function of normal pressure and sliding velocity

At constant sliding velocity; increasing the normal load decreases the friction coefficient. This is due to the shear forces ceasing and the slippage between the interfaces starts. At extreme conditions of loading the rubber detaches as micro particles from the specimen and rolls between the interface and also due to the smearing of water films by the edges of rubber block. This leads to a sudden dip in the friction coefficient values. Figure 43 shows the decreasing wet friction coefficient with increasing vertical load at sliding friction 10mm/s for ES50 and ES100.
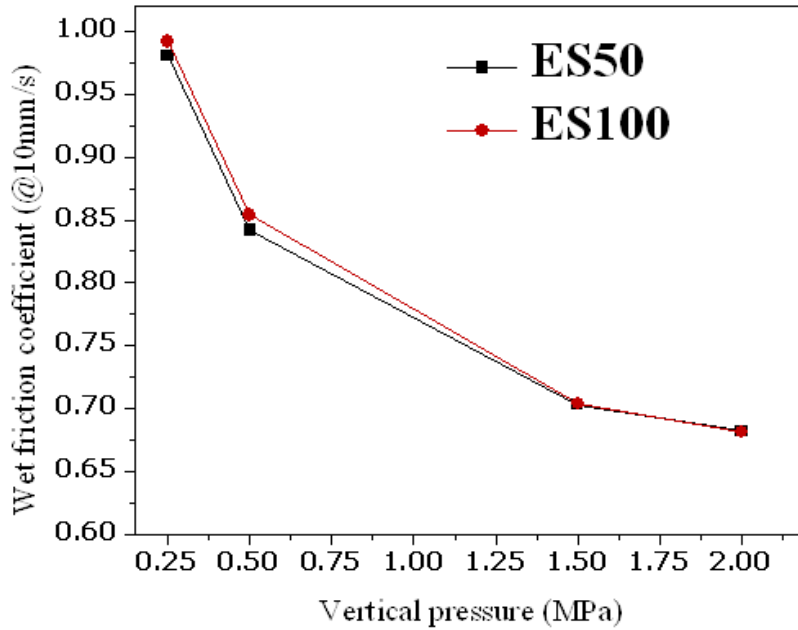
Figure 43: Wet friction coefficient with increasing vertical load at sliding friction 10mm/s

At higher sliding velocities (100mm/s and 1000mm/s) ES100 shows better friction values for lower normal pressures (0.25MPa and 0.5MPa). Increasing the loads reverses the friction performance of the samples. At extreme condition, ES100 sample is undergoing high level of abrasions which is less for ES50. Figure 44 & 45 shows the decreasing wet friction coefficient with increasing vertical load at sliding velocities 100mm/s and 1000mm/s for ES50 and ES100 samples.
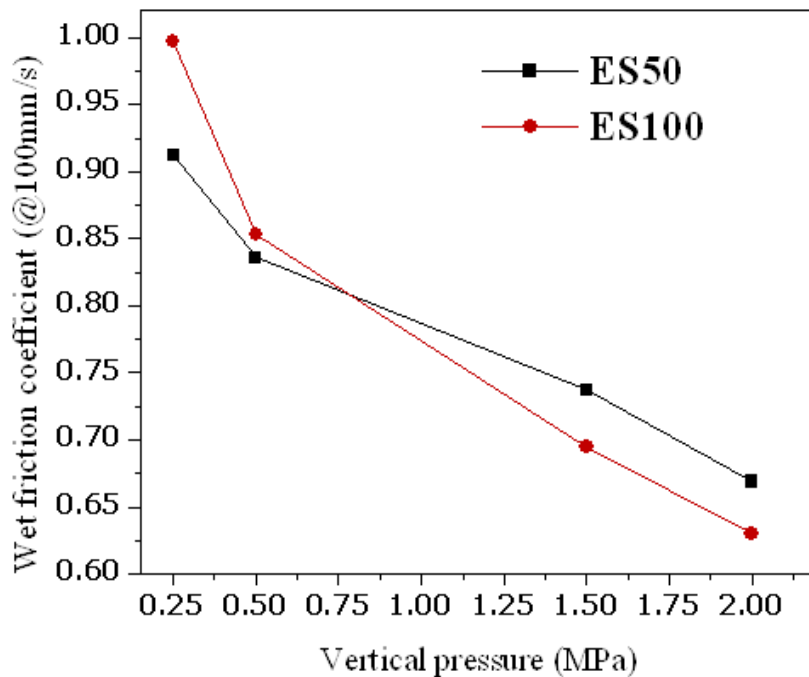
Figure 44: Wet friction coefficient with increasing vertical load at sliding friction 100mm/s
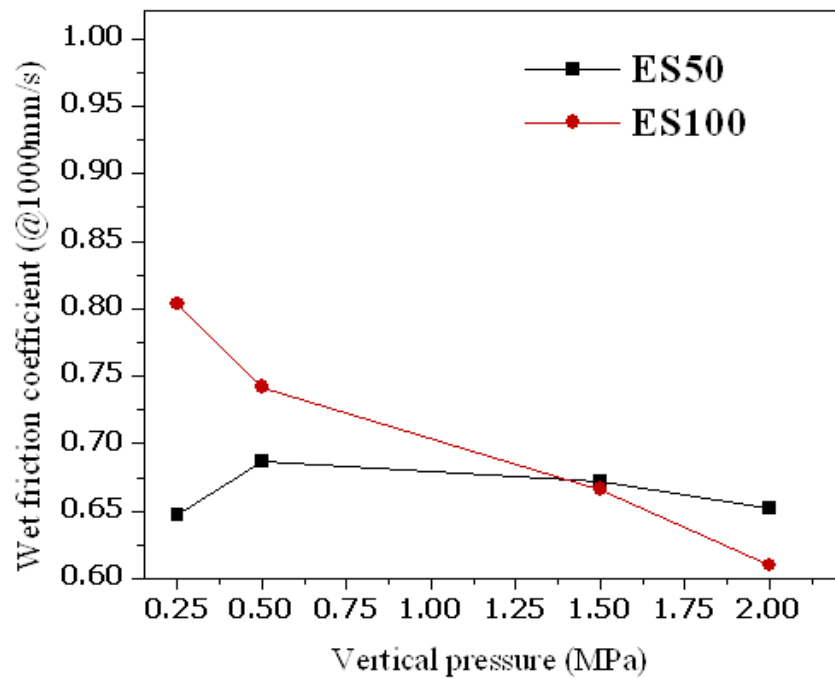
Figure 45: Wet friction coefficient with increasing vertical

load at sliding friction 1000mm/s

Wet Friction as a function of Pressure:

Considering the figure 46, if we derive an exponential model we get a relation with two constants. From the above discussions, it is clear that ES100 is having a better grip in wet conditions. Figure 51 shows the wet friction coefficient fitted to an exponential model.
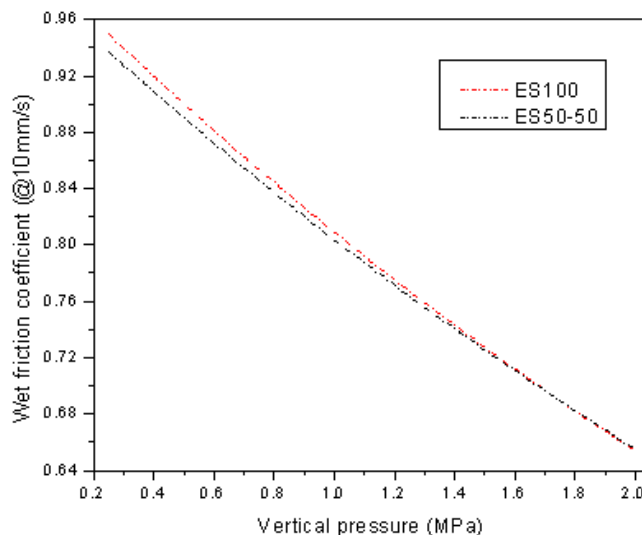
Figure 46: Wet friction coefficient fitted to an exponential

model at sliding velocity 10mm/s

$$\mu_{(Pwet)} = a*e^{bP} \qquad \text{(Generally b varies from -1/3 to -1/9)}$$

Equation y = a*e^{bx} (@10mm/s at various pressure)			
Samples\Parameters	a	b	R^2
ES50	0.986	-0.2045	0.8572
ES100	1.001	-0.2134	0.8753

Table 10: μ_{Pwet} as a function of pressure fitted to an exponential form

Exponential law is valid for the pressure range used for the analysis and the pressure dependent friction is also related to the excitation frequency.

Wet friction as a function of vertical pressure & sliding velocity

Factorial principle equation

The dependence of vertical load and sliding velocities need to be analyzed to determine the wet skid resistance of the tire. Figures 47 and 48 show the frictional coefficient contour plots with respect to load vs. sliding velocity. The contour charts of the samples
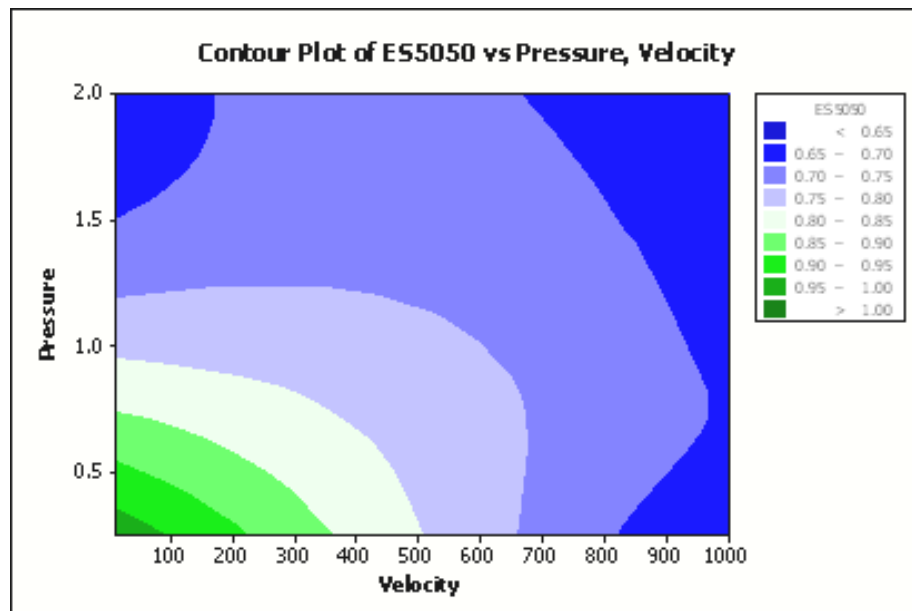
Figure 47: Wet friction coefficient contour plot for ES50

are plotted against the sliding velocity and vertical load.

The rate of change of the friction coefficient with respect to the abscissa and ordinate determines the dependence of the wet friction coefficient

Figure 48: Wet friction coefficient contour plot for ES100

towards the load and sliding velocity.

Numerically this is computed through the multiple regression models. In this model the coefficient of parameter dependence and the product of the parameter dependence are considered. The dependence of load is higher for ES100, as we have seen that the abrasion resistance of the compound is inferior to that of ES50 compound. So if the load increases, the rate of change of wet friction coefficient is also higher.

$$\mu_{(Wet)} = a + b_{(Pressure)} + c_{(Velocity)} + d_{(Pressure*Velocity)}$$

Compound	a	b	c	d
ES50	0.9639	-0.1515	-0.0003	0.0001
ES100	1.0053	-0.1891	-0.0002	0.0001

Table 11: μ_{wet} as a function of pressure and sliding velocity fitted to a multi regression model

The dependence of sliding velocity is more impacting ES50 compound; this is due to less flexible linkages in the matrix, increasing the silica content increases the wet grip properties. The rate of change of wet friction coefficient is more dependent on the change in sliding velocity for ES50 compound.

4.5 Correlation between DMA and LFT results

We have seen that the energy loss (tanδ) at the vicinities of 0°C is considered as the wet grip region. So the area under the tanδ curve is the magnitude considered to correlate with the wet friction coefficients. A single temperature reference is not recommended to predict the wet condition energy loss
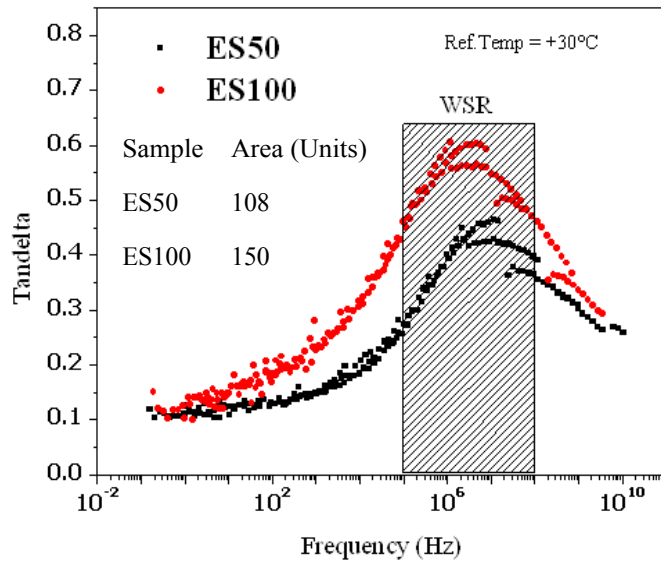
Figure 49: Area under the tanδ curve in WLF master curve for wet grip frequency region

measurements in real situation. So a range is selected starting from -10°C to 20°C; this would give a better insight to the wet grip behaviour. The WLF transform of the samples need to be analyzed at high frequency region ranging from 0.1 MHz till 100 MHz. This
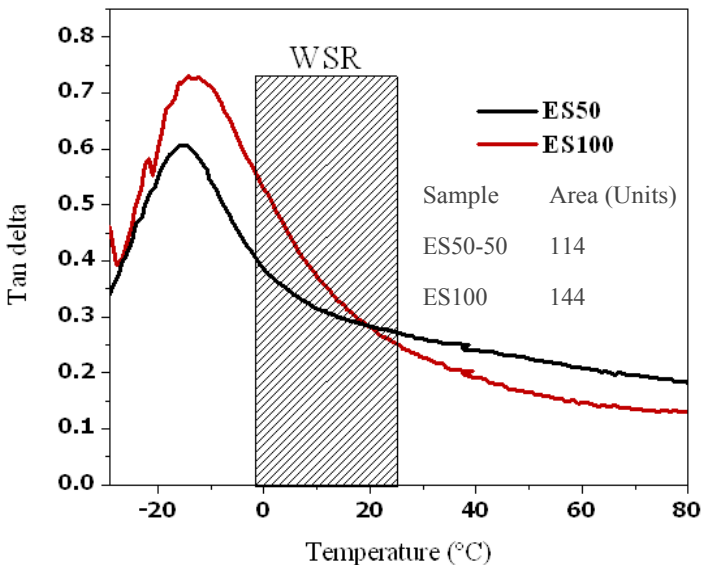
Figure 50: Area under the tanδ curve in temperature sweep for wet grip temperature regime

region predicts the wet grip behaviour. Figure 49 & 50 shows the area under the tan δ curve for temperature and frequency sweep measurements.

From the above figure, it is obvious that the area plot for ES100 is higher than ES50 compound in the temperature sweep measurements. Higher the silica filler content, higher the tanδ at WSR regime. ES50 has an area of 114units where ES100 has an area of 144units in Tsweep measuements. Similar results are observed from the WLF transform curves for both the samples. This ensures that there is a linear relationship among the curves. ES100 has higher control of friction than ES50. This shows the effect of increasing the silica filler loading in-turn increases the tanδ values at higher frequencies. ES100 with 100phr silica shows a distinct increase in the tanδ peaks. The viscoelastic behaviour of the compound counts for the wet grip performance through its damping properties. This is highly correlated to the energy loss (tanδ) of the compound. Silica filled compound shows low tan*δ* at higher temperature and higher tanδ values at lower temperature region. This makes it interesting to see the wet skid performance of the silica compounds.

Area under tan δ curve from temperature & frequency sweep

The wet friction coefficients of both the samples are related to the magnitude of area under the tan δ curve from -10°C to 20°C in the temperature regime and the frequency region ranging from 0.1 MHz to 100 MHz. It is vivid from the above discussions that WSR can be correlated to WLF tan δ curve within the WSR frequency region. In figure 51, ES50 has lower area than the ES100 compound. The wet friction coefficient at extreme loads may be erroneous to build a relation between the tan δ value and the wet grip

performance. So lower loads and its corresponding wet friction coefficients are considered further (0.25 MPa and 0.50 MPa) to analyze and build a relation between the tanδ value and the wet friction coefficient.
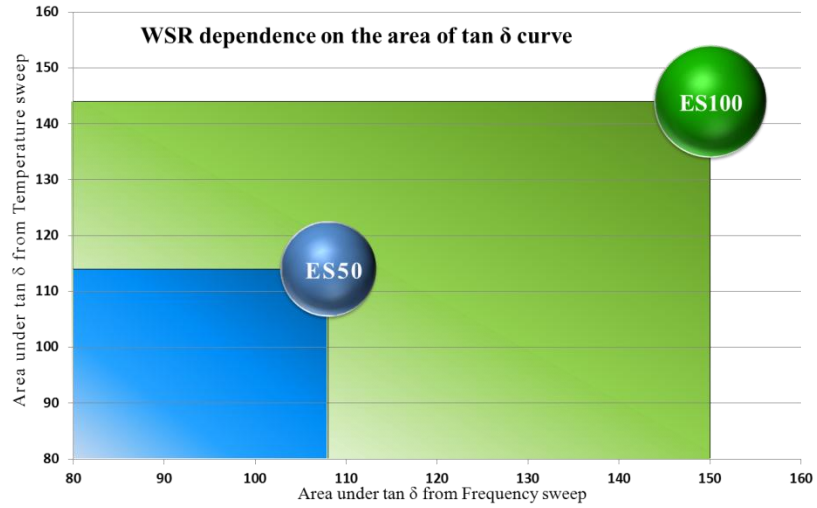

Figure 51: Area under the tanδ curves of ES50 & ES100 in Temperature sweep and WLF transform

Correlation of wet friction coefficient with WLF transform tanδ

Area under the tan δ curve of the wet traction region (0.1MHz to 100MHz) have a linear relationship with wet friction coefficient for lower loads (0.25MPa and 0.5MPa) and for all the sliding velocities (10mm/s, 100mm/s & 1000mm/s) applied for the test. Figure 52 shows the wet friction coefficient dependence at **10mm/s** on the WLF tan δ area. It is
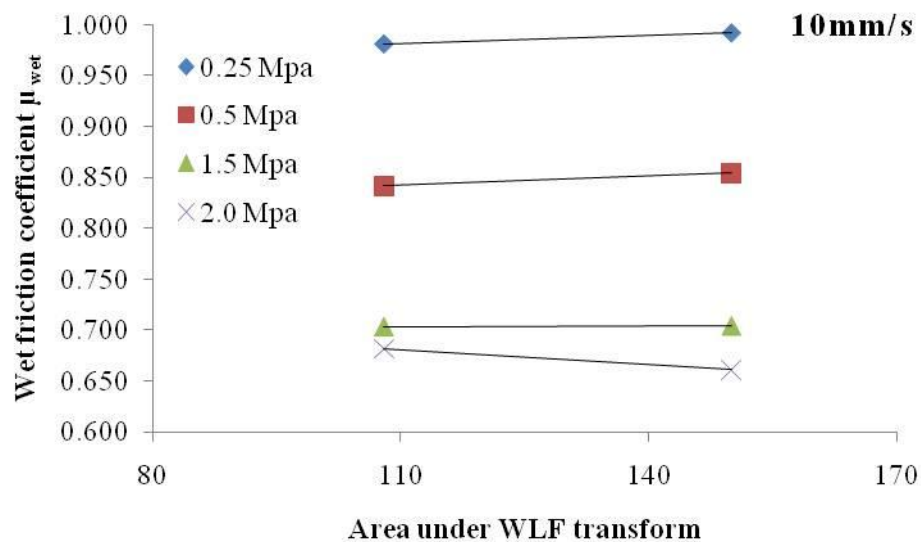
Figure 52: Wet friction coefficient of ES50 & ES100 @10mm/s Vs. Area under tan d in WLF transform

clear from the figure that at lower loads of 0.25MPa and 0.50MPa, there is a linear increase in the wet friction coefficient.

Similarly at 100mm/s the trend seems to be the same, as the area under the tan δ in WLF transform increases, in turn the wet grip enhances. Figure 53 shows the wet friction coefficient dependence at *100mm/s* on the WLF tan δ area.
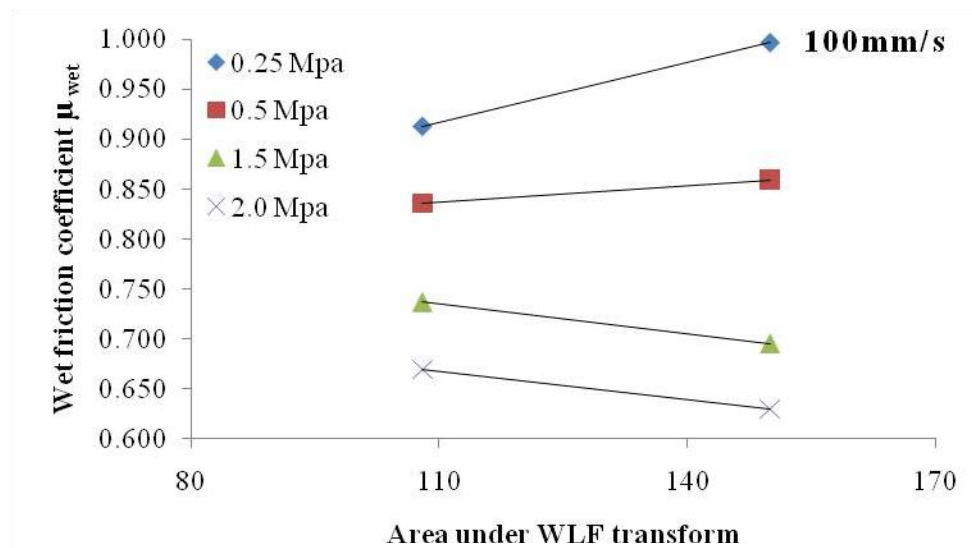
Figure 53: Wet friction coefficient of ES50 & ES100 @100mm/s Vs. Area under tan δ in WLF transform

At extreme sliding velocities, there is an increase in the wet friction which is not linear to the area of tan δ under the WLF transform. Figure 54 shows the wet friction coefficient dependence at *1000mm/s* on the WLF tan δ area. From the sliding velocities of 100mm/s to 1000mm/s
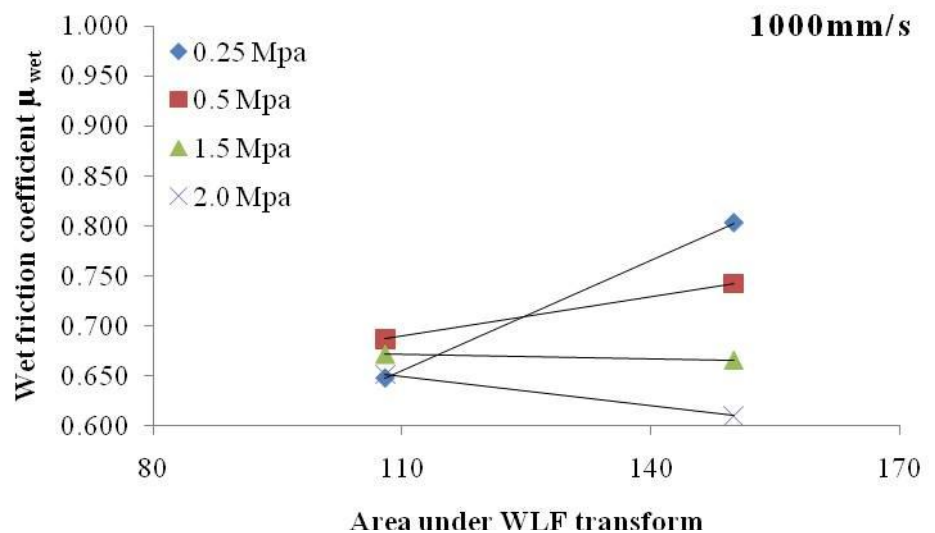
Figure 54: Wet friction coefficient of ES50 & ES100 @1000mm/s Vs. Area under tan δ in WLF transform

there is a drastic reduction in the wet friction coefficient. So differences are found in wet grip performance trend at extreme conditions of loading and sliding velocities.

References:

1 Evans LR and Fultz W C, Rubber World 219:38 (1998).

2 Wolff S and Wang M-J, Rubber chem Technol 65:329 (1992)

3 Boonstra BB, Cochrane h and dannenberg EM, Rubebr Cehm Technol 48:558 (1975)

4 Voet A, Morawski JC and Donnet JB, Rubber Chem Technol 50:342 (1977)

5 Ou Y-C, Yu Z-Z, Vidal A and Donnet JB, Rubber Chem Technol 67:834 (1994)

6. ELSEVIER - Comparison of the mechanical properties at similar hardness level of natural rubber filled with various reinforcing-fillers N. Rattanasom, S. Prasertsri, T. Ruangritnumchai

7. Carbon-silica dual phase filler, a new generation reinforcing agent for rubber part ix. Application to truck tire tread compound, Meng-Jiao Wang*, Ping Zhang and Khaled Mahmud Cabot Corporation, Business & Technology Center 157 Concord Road, Billerica, Massachusetts 01821-7001, USA

8. A. R. Payne, in "Reinforcement of Elastomers", G. Kraus Ed., Interscience Publishers, New York, 1965, Ch. 3.

9. A. R. Payne and R. E. Whittaker, Rubber Chem. Technol., 44, 440 (1971).

10. A. 1. Medalia, Rubber Chem. Technol., 51, 437 (1978).

11. J. R. S. Warring, Trans. Inst. Rubber Ind., 26, 4 (1950).

12. A. R. Payne, J Polym. Sci., 6, 57 (1962).

13. A. R. Payne, Rubber Plast Age, Aug. 963, (1961).

14. The role of material composition in the construction of viscoelastic master curves: silica-filler network effects, By Someyah. Maghami, W. K. Dierkes, T. V. Tolpekina, S. M. Schultz, J. W. M. Noordermeer

15. Wang MJ. Rubber Chem Technol 1998;71(3):520e89

16. A. Le Gal, X. Yang and M. Klüppel, J. Chem. Phys . 123, 1 (2005).

17. M. Wang, R UBBER C HEM. TECHNOL. 71, 520 (1998).

18. J. Fritzsche and M. Klüppel, J. Phys. Condens. Matter. 23,1 (2011).

19. J. Berriot, H. Montes, F. Lequeux, D. Long and P. Sotta, Macromolecules 35, 9756 (2002).

20. L. Guy, S. Daudey, P. Cochet and Y. Bomal, Kautsch. Gummi Kunstst . 62, 383 (2009).

21. G. Heinrich and M. Klüppel, Kautsch. Gummi Kunstst . 57, 452 (2004).

22. Kl¨uppel, M.: Evaluation of viscoelastic master curves of filled elastomers and applications to fracture mechanics. J. Phys. Condens. Matter 21, 035104 (2009)

Chapter 5

Conclusions & Recommendations

Conclusions:

The prediction of wet skid performance of tire tread compounds requires their viscoelastic properties at very high frequencies, in the MHz (0.1 – 100) range and at high deformations need to be determined. However, it is practically not possible to perform such measurements on current dynamic mechanical analyzers. Most commonly the construction of master curves, on basis of the WLF principle is then employed for small strain values in the linear region where the WLF principle is valid.

To produce a proper master curve for a silica-reinforced tire tread compound, both horizontal and vertical shifting need to be applied for the time-temperature superposition. The horizontal shift is based on the WLF principle, making use of the T_{ref} vs. T_g. The vertical shift can be considered as a thermally governed process related to the filler particles as they interact with each other (filler network), and as they are connected to the polymer chains (the filler-polymer interaction). The vertical shift factors for two tire tread compounds with resp. ES50 (50 phr carbon & 50 phr silica) and ES100 (100 phr silica without carbon) showed standard behavior when plotted against inverse of temperature. The high frequency (0.1MHz – 100MHz) or low temperature region (-10°C - 20°C) of the master curve which is considered to represent the wet skid performance of tires,

the loss tangent δ value increases with an increase in the amount of silica filler in a dual phase mixture.

It indicates that increasing the silica filler positively influences the damping properties of the polymer network at lower temperature or at high frequency regime. In the high frequency region of the master curve, this is believed to be responsible for the wet skid performance of tires, the loss tangent δ value increases for ES100 than ES50 with an increase in the amount of silica filler.

Strain sweep measurements performed at different temperatures with strains between 0.01% and 10% on the same two compounds shows a lower Payne effect (Δ E') for ES 100 compared to ES 50. The deformations involved in these Payne measurements are more representative of what happens in real wet traction or skidding of tires.

The friction characteristics from the LFT are best fitting with the lab dynamic analysis. The coefficient of wet friction which is contributed mainly from $F_{Hysteresis}$ revels that increasing the amount of silica filler, increases the wet skid resistance which shows a linear relationship at loads normal loads of 0.25 MPa and 0.50 Mpa applied at slip velocities varying from 10mm/s to 100mm/s. Extreme condition of loading and slip velocities do not follow a linear trend; where in the edge effect, heavy abrasions and less relaxation interval of the rubber matrices of the LFT specimen are happening predominantly.

The dependence of wet friction coefficient (from multi regression model) on load is higher for ES100 sample as more wear and abrasion occur; and the

dependence on sliding velocity is higher for ES50 sample as there are less number of flexible linkages in the compound matrix to hold on to the substrate.

The area under the tan delta shows an attractive correlation with the WSR phenomenon. The increase in the area of tan δ peak in temperature & frequency sweep shows improved WSR capability at loads 0.25MPa & 0.5MPa.

Linear relationship of area from tan δ from temperature sweep and WLF transform optimizes the correlation of WSR capability with the area under tan δ in WLF transform.

From the overall analysis increasing the silica filler dosage eventually increases the *Wet Skid Resistance* of the compound.

The downside of using more silica filler is adversely affecting the wear & abrasion resistance potential of the silica compound design under high loads.

Recommendations:

Varying the LFT specimen geometry; the impact of edge effect could be further investigated by introducing multiple sipes in to the LFT specimen at the contact surface.

The effect of changing the elastomer matrices could be investigated further by introducing the blends of polybutadiene and SBR elastomers on WSR thus improving abrasion resistance.

Appendix

Appendix A: List of Tables

Appendix B: List of Figures

Appendix C: Compounding Formulation

Ingredients	ES50	ES75	ES100
VSL5025 O-SSBR	68.70	68.70	68.70
1783 O-ESBR	68.70	68.70	68.70
HD Silica 7000 GR	46.00	69.00	92.00
Silane X266S	8.00	12.00	16.00
N220 - ISAF	46.00	9.50	0.00
St Acid	2.00	2.00	2.00
Plasticiser VP1454	2.00	2.00	2.00
ZnO	3.00	3.00	3.00
DTPD	0.50	0.50	0.50
Wax	2.00	2.00	2.00
6PPD	2.50	2.50	2.50
Sulfur Insoluble	1.80	1.80	1.80
CBS	1.50	1.50	1.50
DPG	1.50	1.50	1.50

Elastomers in the formulations are designed as 50% oil extended emulsion SBR and 50% oil extended solution SBR. Dual phase filler content is maintained at 100 phr by varying the Carbon black, Silica and Silane coupling agent dosage. For instance ES50 contains 50% silica and 50% carbon black; for ES75 silica is 75% and carbon black is 25% and for ES100 it is 100% silica, with coupling agent.

Appendix D: Specifications of compounding materials

Elastomers

Material Description	Solution SBR 25S/50V/37.5TDAE oil
Manufacturer	Lanxess International S.A,France
Chemical composition	Solution polymerized styrene-butadiene-rubber with 25% bound styrene, 50% vinyl BR as % of total SBR, staining stabilizer, extended with 37.5 phr TDAE oil.
Density	0.950 g/cm3 at 25.0°C
Appearance	Bales
CONTENTS	
Bound styrene content (rhc)	25.00%
C=C Microstructure Vinyl (PH BR)	50.00%
C=C Microstructure Cis (PH BR)	67.00%

Material Description	Emulsion SBR 1783, TDAE oil extended
Manufacturer	Kumho petro chemicals, Korea
Chemical composition	Emulsion polymerised butadiene-styrene copolymer, low nitrosamine, extended with 37.5 phr TDAE oil
Density	0.930 g/cm3 at 25.0°C
Appearance	Bales
CONTENTS	
Bound styrene content (rhc)	23.50%
Oil content	27.30%

Fillers

Material Description	N-220 (ISAF) Carbon black
Manufacturer	Hi-Tech carbon, Gummidipoondi - India
Chemical composition	Amorphous carbon, furnace grade (ISAF), wet/dry pelletized, pelletizing agent
Density	1.800 g/cm3 at 25.0°C
Appearance	Beads
IDENTIFICATION	
DBP absorption	114 ml/100g
Iodine adsorption	121.0 g/kg
Nitrogen surface area (BET)	110.0 m2/g
CTAB	105.0 m2/g
24 M4 DBP absorption	98 ml/100g
Tinting strength	115%

Material Description	ULTRASIL 7000 GR , Highly dispersible silica
Manufacturer	Evonik Industries, GmbH
Chemical composition	Precipitated silica
Density	2.000 g/cm3 at 20°C
Appearance	White granules
IDENTIFICATION	
Nitrogen surface area (BET)	170.0 m2/g
CTAB	160.0 m2/g
pH-value (5g/100ml water)	6.5

Material Description	Silane Coupling agent (X 266 S)
Manufacturer	Evonik Degussa, GmbH
Chemical composition	Mixture of 50 parts Si 266 and 50 parts N330 carbon black
	(Si 266 is a bifunctional, sulfur containing organosilane: Bis -(triethoxysilylpropyl)- disulfide.)
Density	1.310 g/cm3 at 20.0°C

Appearance	Beads
IDENTIFICATION	
Loss on heating at 105°C	<2.00%
Total sulphur content	<8.2.00%

Activators

Material Description	**Stearic acid, rubber grade**
Manufacturer	V.V.F Ltd, Taloja Mumbai
Chemical composition	Mixture of predominantly saturated fatty acids
Density	0.930 g/cm3 at 25.0°C
Appearance	Beads, flakes or granules
CONTENTS	
Refractive index at 70°C	1.43
Acid number	200 mg KOH/g
Saponification number	199 mg KOH/g
Iodine number	8.0 g I2/100g
FATTY ACID FRACTIONS	
Less than C16	7.50%
C16-C20	>90.00%
C21-C22	5.00%
Higher than C22	<1.00%

Material Description	**Zinc oxide indirect**
Manufacturer	J.G Chemicals, Calcutta-India
Chemical composition	Zinc oxide, indirect method of manufacturing
Density	5.600 g/cm3 at 25.0°C
Appearance	White dense powder or granules
CONTENTS	
Ash content at 950°C (as received)	>99.00%
Zinc oxide content (as received)	>99.00%
Cadmium content	250 mg/kg
Copper content	10 mg/kg

Lead content	0.13%
Manganese content	10 mg/kg
Total sulphur content	0..02%
Nitrogen surface area (BET)	5.0 m2/g

Process Aids

Material Description	Plasticiser Structol VP 1454
Manufacturer	Schill & Seilacher, Germany, GmbH
Chemical composition	Compound of fatty acid derivatives
Density	1.000 g/cm3 at 20.0°C
Appearance	Light brown pastilles
CONTENTS	
Drop point	75.0°C
Acid number	80.0 mg KOH/g

Environmental protectors

Material Description	Anti-degradant DTPD
Manufacturer	Lanxess, South Africa
Chemical composition	N'N-diaryl-p-phenylene diamine (Mixture)
Density	1.200 g/cm3 at 25.0°C
Appearance	Brown flakes or beads or pastilles
CONTENTS	
Reactive substance content	>80%
Nitrogen content	10.03%
Iron content	500mg/kg
Diphenyl amine content	5.00%
DTPD	14.00%
DPPD	17.00%
PTPD	35.00%

Material Description	Anti-degradant 6PPD
Manufacturer	Flexys, USA

Chemical composition	N-(1,3-dimethyl butyl)-N'-phenyl p-phenylene diamine
Density	1.000 g/cm3 at 25.0°C
Appearance	Dark purple flakes or pastilles
CONTENTS	
Reactive substance content	95.00%
Nitrogen content	10.00%

Material Description	**Ozone protecting wax PE**
Manufacturer	Paramelt, China
Chemical composition	Mixture of n- and isoparaffinic waxes with 2% polyethylene
Density	0.920 g/cm3 at 20.0°C
Appearance	Pastilles
IDENTIFICATION	
Refractive index at 100°C	1.43
Congealing point	62.0°C
n-Paraffin content (as area % of total paraffin content)	<85.00%

Vulcanization accelerators and Ingredients

Material Description	**Accelerator CBS**
Manufacturer	NOCIL, Mumbai-India
Chemical composition	N-Cyclohexyl-2-Benzothiazole Sulfenamide
Density	1.300 g/cm3 at 25.0°C
Appearance	Light tan to buff colored flakes, pellets, granules or dust suppressed powder
CONTENTS	
Ash content at 750°C	<0.4%
Reactive substance content (Assay)-No additive	>97.00%
Reactive substance content (Assay)- Coated	>95.00%
Moisture	<0.5%
Insoluble in methanol	<0.5%

Material Description	Diphenylguanidine (DPG)
Manufacturer	Hindustan Chemicals Company, Surat
Chemical composition	Diphenylguanidine
Density	1.200 g/cm3 at 25.0°C
Appearance	Granulate, pellets or dust suppressed powder
CONTENTS	
Reactive substance content (Assay)-No additive.	>97.00%
Reactive substance content (Assay)- Coated.	>95.0%
Oil content (for oiled sample)	<2.0%
Insoluble in chloroform (pellets/granulates)	<0.05%

Material Description	Soluble Sulphur, semi-coarse, 0.5% Oil Treated
Manufacturer	Jain Chemicals,Kanpur
Chemical composition	Ground rhombic sulfur with 0.5% naphthenic oil added
Density	2.050 g/cm3 at 25.0°C
Appearance	Powder oil treated
CONTENTS	
Sieve residue on 0.075 mm	6.00%
Total sulphur content (as % of non-oiled sulphur)	>99.00%
Oil content	0.50%
Matter insoluble in Toluene	<0.5%